

**SPATIAL DISTRIBUTION OF CONTAMINANT CONCENTRATIONS IN THE
ST. MARYS RIVER**

by

Christian John Krnic

A Major Research Paper

presented to Ryerson University

in partial fulfillment of the requirements for the degree of

Master of Spatial Analysis (MSA)

Toronto, Ontario, Canada

© Christian Krnic 2012

Author's Declaration

I hereby declare that I am the sole author of this major research paper. This is a true copy of the major research paper, including any required final revisions, as accepted by my examiners.

I authorize Ryerson University to lend this research paper to other institutions or individuals for the purpose of scholarly research.

I further authorize Ryerson University to reproduce this major research paper by photocopying or by other means, in total or in part, at the request of other institutions or individuals for the purpose of scholarly research.

I understand that my major research paper may be made electronically available to the public.

Abstract

The St. Marys River is listed as an Area of Concern (AOC) in the Great Lakes Water Quality Agreement between Canada and the United States. The river system has been severely impacted by modifications to its hydrology, as well as local industrial and municipal discharges. Remedial Action Plans (RAPs) by the Ontario Ministry of the Environment have been developed since 1988. Anthracene, flourene, pyrene, total polycyclic aromatic hydrocarbons (PAHs), and total polychlorinated biphenyls (PCBs) concentrations at depths of 0-5 cm and 5-10 cm in a small portion of the St. Marys River were analyzed in this study. The contamination data were provided by Environment Canada through the Canada Centre for Inland Waters. Ordinary kriging and inverse distance weighting (IDW) spatial interpolation techniques were used to calculate and compare estimates between sample locations for the contaminants. The results show that the 0-5 cm depth is less contaminated than the 5-10 cm depth. The lower contamination levels in the top layer may signify that historical contamination was greater than present day contamination. Overall, the contamination concentrations are all concerning, as all but two Total PCBs samples are categorized above the Threshold Effect Level (TEL) designated by the Canadian Council of Ministers of the Environment. The two interpolation techniques had similar cross validation statistics however the prediction surface maps produced significantly different patterns in some cases. The findings may assist in restoring the natural habitat of the river and to determine contamination sources.

Acknowledgements

I would like to acknowledge the support and guidance of my supervisor, Dr. Wayne Forsythe.

A special thanks to Debbie Burniston from the Canada Centre for Inland Waters for providing the original data files which made this research possible.

Dedication

This work is dedicated to my family, friends, and the Geomatics Centre at the MOE for their support and motivation.

Table of Contents

Author’s Declaration.....	ii
Abstract.....	iii
Acknowledgements.....	iv
Dedication.....	v
Table of Contents.....	vi
List of Tables.....	viii
List of Figures.....	ix
List of Acronyms.....	x
CHAPTER 1: INTRODUCTION	1
1.1 Polycyclic Aromatic Hydrocarbons.....	4
1.2 Polychlorinated Biphenyls.....	5
1.3 Spatial Interpolation Techniques	7
1.4 Study Area	10
1.5 TEL and PEL.....	11
1.6 Research Objectives.....	12
CHAPTER 2: BACKGROUND	13
2.1 History of St. Marys River Contamination	13
2.2 Spatial Interpolation Techniques in Contamination Studies	15
2.3 PCB and PAH Research.....	18
CHAPTER 3: DATA AND METHODOLOGY.....	20
3.1 Data.....	20
3.2 Methodology.....	23
3.3 Cross Validation Statistics.....	27
3.4 Log-Transformations	29
CHAPTER 4: ANALYSIS	33
4.1 Total PCBs	35
4.2 Anthracene.....	37
4.3 Flourene.....	42
4.4 Pyrene.....	46
4.5 Total PAHs	50

CHAPTER 5: CONCLUSIONS.....	55
5.1 Recommendations and Further Research.....	57
REFERENCES.....	58

List of Tables

Table 1.1: Chronology of St. Marys River History	3
Table 1.2: Table of Contaminants and Federal Guidelines	12
Table 3.1: Contaminant descriptive statistics for depths of 0-5cm.	22
Table 3.2: Contaminant descriptive statistics for depths of 5-10cm.	22
Table 3.3: Total PCBs descriptive statistics for depths of 0-10cm.	22
Table 3.4: Contaminant MPE and RMSPE statistics for depths of 0-5cm using ordinary kriging.....	31
Table 3.5: Contaminant MPE and RMSPE statistics for depths of 5-10cm using ordinary kriging.....	31
Table 3.6: Total PCBs MPE and RMSPE statistics for depths of 0-10cm using ordinary kriging.....	32
Table 3.7: Contaminant MPE and RMSPE statistics for depths of 0-5cm using IDW.....	32
Table 3.8: Contaminant MPE and RMSPE statistics for depths of 5-10cm using IDW. ...	32
Table 3.9: Total PCBs MPE and RMSPE statistics for depths of 0-10cm using IDW.	32
Table 4.1: Number of Sediment Sampling Locations in Relation to TEL and PEL Categories	33

List of Figures

Figure 1.1: Location of the St. Marys River	1
Figure 1.2: Great Lakes Areas of Concern that are shared between Canada and the USA. 4	
Figure 1.3: Study area in proximity to Sault Ste. Marie.	10
Figure 3.1: Sample point distribution within the study area.	21
Figure 3.2: Methodology workflow.	24
Figure 4.1.1: Distribution of Total PCBs sample point concentrations within the study area at a depth of 0-10 cm.	35
Figure 4.1.2: Ordinary kriging Total PCBs log-normal concentrations at a depth of 0-10 cm.	36
Figure 4.1.3: IDW Total PCBs log-normal concentrations at a depth of 0-10 cm.	37
Figure 4.2.1: Distribution of anthracene sample point concentrations within the study area.	38
Figure 4.2.2: Ordinary kriging anthracene log-normal concentrations within the study area.	40
Figure 4.2.3: IDW anthracene log-normal concentrations within the study area.	41
Figure 4.3.1: Distribution of flourene sample point concentrations within the study area.	43
Figure 4.3.2: Ordinary kriging flourene log-normal concentrations within the study area.	44
Figure 4.3.3: IDW flourene log-normal concentrations within the study area.	45
Figure 4.4.1: Distribution of pyrene sample point concentrations within the study area.	47
Figure 4.4.2: Ordinary kriging pyrene log-normal concentrations within the study area.	48
Figure 4.4.3: IDW pyrene log-normal concentrations within the study area.	49
Figure 4.5.1: Distribution of Total PAHs sample point concentrations within the study area.	51
Figure 4.5.2: Ordinary kriging Total PAHs log-normal concentrations within the study area.	52
Figure 4.5.3: IDW Total PAHs log-normal concentrations within the study area.	53

List of Acronyms

AOC	Area of Concern
CCME	Canadian Council of Ministers of the Environment
EC	Environment Canada
GIS	Geographic Information Systems
IDW	Inverse Distance Weighting
MPE	Mean Prediction Error
MOE	Ontario Ministry of the Environment
PAHs	Polycyclic Aromatic Hydrocarbons
PCBs	Polychlorinated Biphenyls
PER	Possible Effect Range
PEL	Probable Effect Level
POPs	Persistent Organic Pollutants
PSQG	Provincial Sediment Quality Guidelines
RAP	Remedial Action Plan
RMSPE	Root Mean Squared Prediction Error
SRMSPE	Standardized Root Mean Squared Prediction Error
TEF	Toxic Equivalency Factors
TEL	Threshold Effect Level
UGLCCS	Upper Great Lakes Connecting Channel Study

CHAPTER 1: INTRODUCTION

The St. Marys River flows over 100 kilometres as Lake Superior's surface outlet to Lake Huron, forming a natural international boundary between Canada and the United States of America. The river is shared between the eastern end of the State of Michigan and a north western section of the Province of Ontario (Figure 1.1).

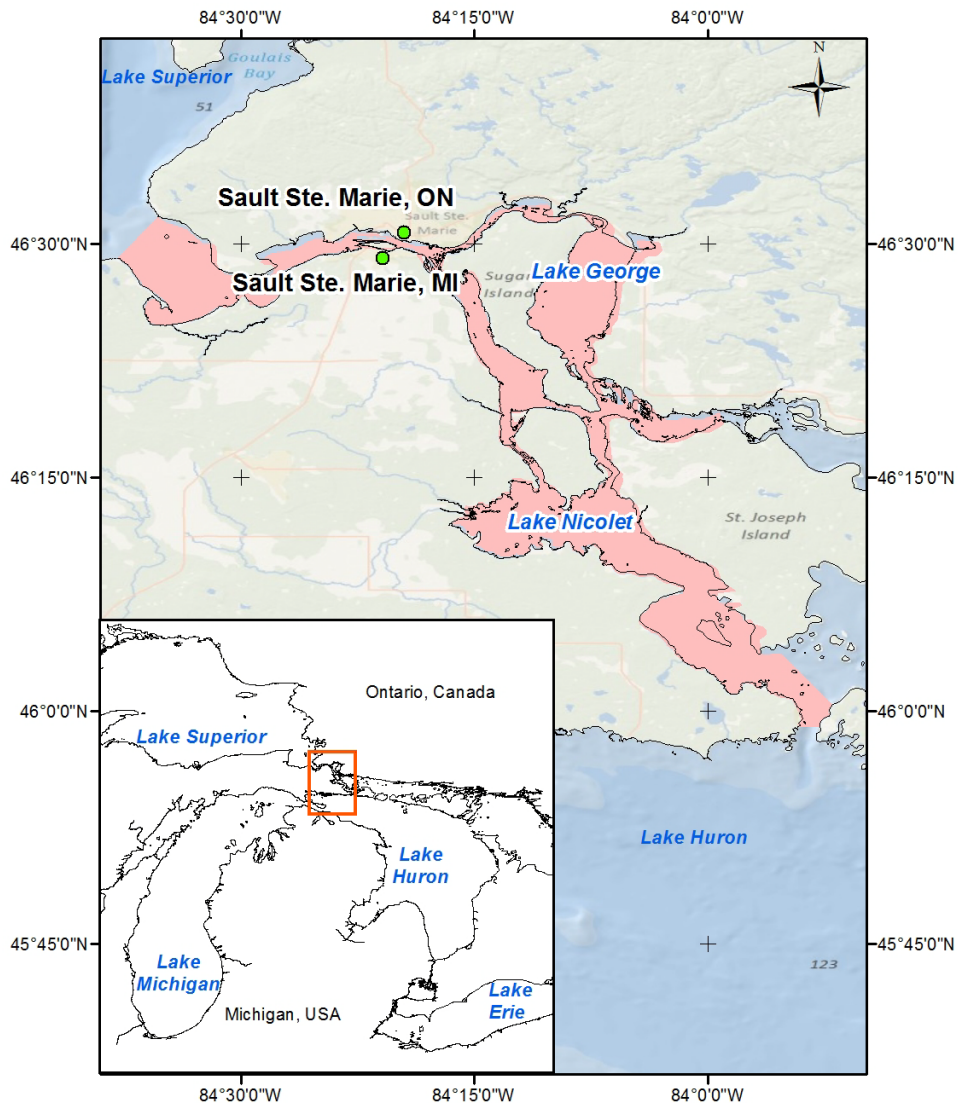


Figure 1.1 – Location of the St. Marys River. The red area within the St. Marys River represents the St. Marys River Area of Concern (AOC).

In addition to providing political boundaries, the river plays a vital role in the local and national economies of both countries, as part of a series of Great Lakes connecting channels. As seen in Table 1.1, the St. Marys River has historically been, and continues to be, a vital source of shipping and industry to this region (Arbic, 2003; Keller et al., 2011). The two largest cities on the river are the twin cities of Sault Ste Marie, across from one another on opposite sides of the international border. The Soo Locks receive over 10,000 vessel passages, carrying over 80 million tons of goods a year (Figure 1.3), making it one of the busiest locks in the world (Moerke and Werner, 2011).

Impacts from nearly 200 years of industrialization, navigational construction and loss of habitat in the urbanized areas of the river have led to environmental degradation and listing of the river as a Great Lakes Area of Concern (AOC) (Figure 1.2) (RAP, 1992). Due to the rich biological diversity, the river was identified as a priority for conservation and remediation (Moerke and Werner, 2011). AOCs are designated areas that show severe environmental degradation. There are a total of 43 AOCs within the Great Lakes, 26 in the USA, 12 in Canada, and an additional five shared between the two countries (Figure 1.2) (GLWQA, 1987; Keller et al., 2011; RAP, 1992; RAP, 2002).

By the 1970s, the river became severely polluted and required significant remediation (RAP, 1992; RAP, 2002; Ripley et al., 2011), even though two major developments were completed after: the 1982 hydroelectric plant expansion and the 1986 berm construction as seen Table 1.1.

Table 1.1: Chronology of engineering events associated with the development of the St. Marys Rapids and River. Adapted from Koshinsky and Edwards (1983); retrieved from Ripley et al. (2011).

Year	Event
1797	Navigation Lock 11.5 m long constructed on Canadian side.
1822	Raceway and sawmill built on American side by U.S. Army.
1839	Navigation canal started on American side, construction later aborted.
1855	Navigation lock completed on American side.
1859	Dredging of Lake George Channel completed.
1881	Weitzel Lock on American side completed.
1887	Lock of 1855 dismantled and replaced by larger set.
1888	International railway bridge completed.
1894	Dredging of Lake Nicolet Channel completed.
1896	Canadian Government canal and lock completed; old State locks on American side replaced by Poe Lock.
1901	Construction of compensating works begun.
1902	Edison Hydroelectric Canal and power plant completed; canal diverted enough water to operate 41 turbines, each using approximately 10.6 m ³ /s.
1908	Ship canal through West Neebish Rapids (rock cut) completed.
1914	Davish Lock on American side completed.
1915	Additional 37 turbines added to Edison Hydroelectric plant.
1916	Hydroelectric canal and plant completed on Canadian side
1919	Sabin Lock on American side completed.
1921	Construction of compensating works completed.
1927	Widening of Middle Neebish Channel completed.
1933	Widening of canal through West Neebish Rapids completed.
1943	MacArthur Lock on American side completed, replacing Weitzel Lock. Hydroelectric plant on Canadian side redeveloped and capacity increased from
1982	510 to 1076 m ³ /s.
1986	Berm constructed to maintain water level for fish habitat in rapids.



Figure 1.2: Great Lakes Areas of Concern that are shared between Canada and the USA (highlighted in red).

1.1 Polycyclic Aromatic Hydrocarbons

Total polycyclic aromatic hydrocarbons (PAHs) are prominent hydrophobic organic contaminants (HOCs) and persistent organic pollutants (POPs) that are ubiquitous (De La Torre-Roche et al., 2009; Foster and Cu, 2008). Researchers have found PAHs globally, even in the most remote areas of the Arctic (De La Torre-Roche et al., 2009). HOCs are a serious concern to water quality managers and scientists as they pose a threat to human and ecosystem health through dietary or inhalation exposures at low concentrations in contaminated food, water, sediment, and air (Foster and Cui, 2008). Direct human and animal adverse biological effects of PAHs include acute toxicity,

developmental and reproductive toxicity, mutagenicity and carcinogenicity (De La Torre-Roche et al., 2009; Feo et al., 2011; Sower and Anderson, 2008).

PAHs can be released to the environment through (1) pyrogenic activities - combustion of organic materials during industrial activities, residential heating, power generation, incineration, vehicle emissions; (2) petrogenic activities - emission from petrochemical refining and chemical manufacturing; or, (3) occur naturally (i.e., volcanic activity). They are most commonly formed during incomplete burning of oil, wood, garbage, or other organic substances (tobacco, charbroiled meat) (De La Torre-Roche et al., 2009; Feo et al., 2011).

Generally, PAHs from petrogenic sources have a lower molecular weight (2-3 rings), where pyrogenic are heavier (4-6 rings). The heavier PAHs tend to settle more easily near the point of emission as lighter PAHs can easily re-suspend and can travel further away from point sources (De La Torre Roche et al., 2009). PAHs that are considered priority pollutants by the USEPA Clean Water Act (included in this study) are pyrene and anthracene (Feo et al., 2011). Flourene is obtained from coal tar. It poses environmental threats as it is insoluble in water, contributing to bioaccumulation in the ecosystem (De La Torre Roche et al., 2009).

1.2 Polychlorinated Biphenyls

Similarly to PAHs, polychlorinated biphenyls (PCBs) are prominent HOCs and are found ubiquitously around the globe (Foster and Cui, 2008). A substantial amount of PCBs generated historically are capable of being predominant in the environment for several generations (Foster and Cui, 2008). PCBs were manufactured globally by various

industries since the 1920s. PCBs were widely used as dielectric and coolant fluids, mainly for transformers, capacitors, and electric motors, and as plasticizers in paints and rubber sealants (Feo et al., 2011; Salihoglu et al., 2011). The USA and Canada assessed PCB contamination in various sites and issued manufacturing bans in the late 1970s with hefty penalties for any industry caught using them (Breivik et al., 2002; Heidtke et al., 2006). The use of PCBs was banned in the European Union (EU) in 1985 (Feo et al., 2011) and in the 1990s by former USSR states (Breivik et al., 2002). The global production of PCBs in 2002 was estimated to be at 1.5 million t, with 650 kt produced in the USA alone (Breivik et al., 2002).

PCBs are unreactive and have long lives in the body, with first-order estimates of over 25 years for some recalcitrant congeners. This causes bioaccumulation residues to increase with age in large predatory species in aquatic ecosystems (Breivik et al., 2002; Foster and Cui, 2008). Although there might not be immediate substantial toxicity risk to a benthic organism, concerns will always remain over the bioaccumulation potential of PCBs (Foster and Cui, 2008).

Although direct human acute toxicity is rare, chronic low-level exposures can pose the greatest risk, which can cause cancer and developmental abnormalities (Foster and Cui, 2008). Researchers have recently discovered that certain PCBs act similar in nature to dioxin and appear to pose similar risks to both humans and animals (Feo et al., 2011; Solihoglu et al., 2011).

1.3 Spatial Interpolation Techniques

The spatial and temporal occurrence of Total PCBs and Total PAHs contamination must be known to allow more accurate remediation efforts to be implemented (Sower and Anderson, 2008). Spatial interpolation is a method of estimating variables at unobserved locations as well as re-estimating variables at observed locations (Dille et al., 2002). Sample observations should be represented at an operational scale that adequately captures the spatial variability across the region of interest (Palmer et al., 2009). Inverse distance weighting (IDW) and ordinary kriging are the most frequently used spatial interpolation methods in academic studies (Li and Heap, 2011).

Spatial interpolation methods can be implemented either (1) globally - large scale heterogeneity – model is constructed from all observations and estimated values at any point in the study area are dependent on all sampling points; or (2) locally – small scale heterogeneity – model is constructed from all observations, but only a subset of data is used to estimate values (Dille et al., 2002). This provides researchers great variability, as sample collection can vary depending on geographical, economical, and social constraints. In addition, Li and Heap (2011) summarized a list of factors that affect the performance of spatial interpolation methods, including: sampling density, sample spatial distribution, sample clustering, surface type, data variance, data normality, quality of secondary information, stratification, and grid size.

Spatial interpolation techniques can be categorized as one of two models: deterministic to interpolate point information using similarities between measured points

and fitting a smoothing curve along the measured points or stochastic modeling using parameters derived from semivariograms (Joseph et al., 2010)

The theory behind interpolation and extrapolation by kriging was developed by the French mathematician Georges Matheron (Clark, 1979). The technique and thereby the name of the technique was based on the 1960s Master's thesis of Daniel Gerhardus Krige, a South African Mining Engineer. Krige pioneered the technique by plotting the distance-weighted average gold grades, at the Witwatersrand reef complex in South Africa (Clark, 1979; Houlding, 2000; Johnston et al., 2001). Although the geospatial technique was originally developed for the mining industry, it has since been developed effectively to be used in sediment concentration estimation (Forsythe et al., 2010; Gawedzki and Forsythe, 2012).

Kriging is a group of spatial interpolation methods for assigning a value of a random field to an unsampled location, based on the measured values of the random field at nearby locations (Gu et al., 2012; Li and Heap, 2008; Xie et al., 2011). The kriging tool is known as the best unbiased linear estimator for unsampled sites (Kazemi and Hosseini, 2011; Palmer et al., 2009). Ordinary kriging is the most general and widely used of the kriging methods and is the default because it assumes the constant mean is unknown. This is a reasonable assumption unless there is a scientific reason to reject it (ESRI, 2010; Li and Heap, 2011; Merwade, 2009). The general formula is formed as a weighted sum of the data:

$$\hat{Z}(s_0) = \sum_{i=1}^N \lambda_i Z(s_i) \quad (1)$$

where $Z(s_i)$ is the measured value at the i th location; λ_i is an unknown weight for the measured value at the i th location; s_0 is the prediction location; and N is the number of measured values (Clark, 1979; Li and Heap, 2011; Palmer et al., 2009).

A preliminary IDW methodology was developed by a group of scientists at the Harvard Laboratory for Computer Graphics and Spatial analysis, to produce an improved computer mapping program and improve interpolations in the 1960s. In 1968, Donald Shepard, a Harvard undergraduate student, overhauled the IDW methodology that is still used now (Shepard, 1968). IDW assumes that the predictions are a linear combination of available data, and greater weighting values are assigned to values closer to the interpolated point (Gu et al., 2012; Li and Heap, 2008; Xie et al., 2011). As the distance increases between the observed sample locations and the prediction location, the weight the observed data point will have on the prediction decreases exponentially (Palmer et al., 2009).

The weight for each sampled location is inversely proportional to a power of its distance from the location being estimated:

$$f(x, y) = \frac{\left[\sum_{i=1}^N w(d)z_i \right]}{\left[\sum_{i=1}^N w(d_i) \right]} \quad (2)$$

where $f(x,y)$ is the interpolated value at point (x,y) ; $w(d_i)$ is the weighting function; z_i is the data value at point i ; and d_i is the distance from point (x,y) (Isaaks and Srivastava, 1989; Lam, 1983; Salihoglu et al., 2011). The weighted function (w) adjusts the weights to be inversely proportional to any power of the distance. The larger the power (exponent

used), the smaller the effect of distance on the weights (Dille et al., 2002; Isaaks and Srivastava, 1989; Lam, 1983).

1.4 Study Area

This study area is located in the St. Marys River approximately 200 metres south of the Algoma University campus, 15 metres south of Shingwauk Island, 15 metres east of Topsail Island and approximately 4 kilometres east of the Sault Ship Canal (Figure 1.3). This portion of the river is immediately downstream from the twin cities of Sault Ste. Marie, and is at the most eastern part of the river before it splits into Lake Nicolet and Lake George (see Figure 1.3).



Figure 1.3: Study area in proximity to Sault Ste. Marie. The orange rectangle indicates the study area boundaries.

1.5 TEL and PEL

This study uses the Threshold Effect Level (TEL) and the Probable Effect Level (PEL) as freshwater sediment quality indicators provided by the Canadian Council of Ministers of the Environment (CCME). The TEL is the concentration level where fewer than 25 percent of the adverse biological effects are encountered for organisms living in, or having direct contact with the contaminated sediments. The PEL is the concentration level where more than 50 percent of the adverse biological effects are encountered for organisms living in, or having direct contact with the contaminated sediments (Canadian Council of Ministers of the Environment, 2001; Keller et al., 2011).

Previous studies used other variations of sediment quality guidelines, such as the Lowest Effect Level (LEL) of Ontario Ministry of the Environment's (MOE) Provincial Sediment Quality Guidelines (PSQG) while examining PCB accumulation in osprey (Solla and Martin, 2008); or using the World Health Organization's (WHO) Toxic Equivalency Factors (TEFs) both for examining PAH and PCB spatial distribution patterns in Naples, Italy (Feo et al., 2009) and soil borne PAHs in El Paso, Texas (De La Torre-Roche et al., 2009). The TEL and PEL guidelines provided by the CCME were used in several Great Lakes studies (Forsythe and Marvin, 2009; Gawedzki and Forsythe, 2012; Jakubek and Forsythe, 2004; Keller et al., 2011; Rodriguez, 2009).

The three class range groups examined in this study include contaminants (1) below the TEL, (2) between the TEL and PEL (as Rodriguez, 2009 identified as the Possible Effect Range (PER)), (3) and above the PEL. The CCME PEL and TEL values for Total PCBs, anthracene, flourene, pyrene, and Total PAHs are found in Table 1.2.

Table 1.2: Table of Contaminants and Federal Guidelines; Source: Canadian Council of Ministers of the Environment, 1999

Contaminant	TEL	PEL
<i>Total PCBs</i>	34.1 ng/g	277 ng/g
<i>Anthracene</i>	46.9 ng/g	245 ng/g
<i>Flourene</i>	21.2 ng/g	144 ng/g
<i>Pyrene</i>	53 ng/g	875 ng/g
<i>Total PAHs</i>	4,000 ng/g	200,000 ng/g

1.6 Research Objectives

The primary objective of this study is to compare and assess the results of ordinary kriging and IDW spatial interpolation methods to determine which is most appropriate for small scale studies. In order to achieve the primary objective, the following secondary objectives will be completed:

1. Assess and compare the spatial distributions of anthracene, flouene, pyrene, Total PCBs and Total PAHs present;
2. Identify the areas within the study that have pollution levels
 - a. below the TEL,
 - b. between the TEL and the PEL,
 - c. and above the PEL;
3. Produce prediction surface maps and cross validation statistics for the distribution of the above sediment contaminant concentrations.

CHAPTER 2: BACKGROUND

2.1 History of St. Marys River Contamination

The St. Marys River has a long history of heavy industrial activity located in the vicinity (refer to Table 1.1). Industrialists envisioned that any number of factories could be built using cheap electricity generated by hydropower at Sault Ste. Marie, with Lake Superior acting as “the largest millpond in the world” (Arbic, 2003). Although much of the river contains important fish and wildlife habitat, including mostly intact coastal wetlands, the urban areas of the upper St. Marys River have been impacted over the past 100+ years by industrial and navigational development (Keller et al., 2011; RAP, 2002; Ripley et al., 2011).

Enforcement of environmental regulations enacted in Canada and the U.S., investments in pollution control technology by industry and the municipalities, and improved fisheries management for invasive species have resulted in improved environmental conditions, however legacy impacts remain (RAP, 2002; Ripley et al., 2011). For example, before installation of secondary treatment processes in the 1990s, St. Marys Paper released suspended solids (bark clay, wood), cooling water and soluble organic compounds through one direct outfall located in the tailrace of the adjacent hydroelectric plant (Keller et al., 2011; RAP, 1992).

The on-going Remedial Action Plan (RAP) process provides a framework for continued environmental improvements (RAP, 2002; Ripley et al., 2011). The Stage I RAP issued in 1992 identified the sources and magnitudes of impairments to the river while the Stage II RAP issued in 2002 identified many actions needed to remove the

beneficial use impairments (Keller et al., 2011; RAP, 2002). The river is currently in Stage III, as it is continuously monitored for confirmation that remedial strategies and restoration initiatives are being implemented and effective (SSMRCA, 2012). A plan to address contaminated sediments remaining in the river is currently being written. Surveys of the fish and wildlife population are monitored to determine environmental impacts. Improvements to wastewater treatment plants on both sides of the river have also resulted in improved water quality (Arbic, 2003; SSMRCA, 2012).

The impacts of industrial discharges to the St. Marys River in the twentieth century were documented with the Upper Great Lakes Connecting Channels Study (UGLCCS, 1988), commissioned by the Canadian and U.S. governments in 1984. Results of the study completed in 1988, outlined the extent of industrial discharges at the time, impact to biota and the delineation of contaminated sediments on the bottom of the river. Levels of Total PAHs assumed to originate from the steelmaking process, surged in the 1940s, and peaked in the late 1960s and early 1970s (Arbic, 2003; Keller et al., 2011; UGLCCS, 1988).

Although high concentrations of certain metals have been found throughout sediments in the St. Marys River, the majority of contaminated sediments occur in deposition zones on the Canadian side of the river, in areas downstream of point sources. The areas of heaviest contamination are identified as the Algoma Steel Slip and the area from Bellevue Marine Park to Little Lake George (Arbic, 2003; Keller et al., 2011; Ripley et al., 2011). The study area in this paper is located within this portion of the St. Marys River. This research will analyze the concentrations of anthracene, flourene, pyrene, Total PAHs, and Total PCBs while comparing the ordinary kriging and IDW

spatial interpolation techniques. The techniques will identify areas of higher concentrations and the contaminant patterns could 'point' to the contributors.

2.2 Spatial Interpolation Techniques in Contamination Studies

It is essential for scientists to understand the sources, distribution and sediment geochemistry of contaminants that can pose a risk to human and environmental health in order to establish proper management practices and public policies (Foster and Cui, 2008). Spatial Interpolation techniques have been used in sediment contamination studies for analyzing PAHs and Total PCBs (Forsythe and Marvin, 2005; Gawedzki and Forsythe, 2011; Jakubek et al., 2004; Lambert et al., 2011; Nichols et al., 1991; Venkatesan, 2010; Xie et al., 2011). Spatial interpolation methods provide an estimation tool for values at unsampled sites using data from point observation samples (Li and Heap, 2011; Xie et al., 2011). Scientists need the data to be spatially accurate and continuous in the study area to make justified interpretations and assessments (Forsythe and Marvin, 2005; Keller et al., 2011; Nichols et al., 1991; Xie et al., 2011).

In IDW, the weight depends solely on the distance to the prediction location. However, with the kriging method, the weights are based not only on the distance between the measured points and the prediction location, but also on the overall spatial arrangement of the measured points (ESRI, 2010). IDW assumes that the predictions are a linear combination of available data, and greater weighting values are assigned to values closer to the interpolated point (Gu et al., 2012; Li and Heap, 2008; Xie et al., 2011). As the distance increases between the observed sample locations and the

prediction location, the weight the observed data point will have on the prediction decreases exponentially (Palmer et al., 2009).

Rodriguez (2009) used kriging in his research of mercury and lead contamination in the Buffalo River. He performed two spatial prediction error maps for the contaminants, (1) breaking up the river into three segments, performing individual kriging prediction maps on each, and (2) performing a single kriging prediction map on the entire river. The results showed that the maps did not differ much since the technique assumes spatial autocorrelation exists within the sample points.

Dille et al. (2002) compared the results of ordinary kriging and IDW interpolators for small sampled weed (hemp dogbane, common sunflower, foxtail species, and velvet leaf) distribution maps within a large scale area. They concluded that IDW and ordinary kriging gave equal precision among interpolation methods for high infestation level populations and that they both produced low levels of precision and global estimation. Specifically, they found that for foxtail weed species, IDW resulted in the smallest root mean square (RMS) values across interpolators and prediction data subsets. IDW and ordinary kriging methods resulted in the smallest RMS values for velvet leaf weed species.

Cross validation statistics provide a standard medium for researchers to compare different techniques using statistics such as root mean square prediction error (RMSPE) and the mean prediction error (MPE). The root mean square prediction error (SRMSPE) value is important as it provides a method to assess variability (Jakubek and Forsythe, 2004). Only the ordinary kriging SRMSPE values are assessed since they are not

calculated for IDW. Li and Heap (2011) provided a comparative study examining the cross validation results from various studies in determining which spatial interpolation method is most appropriate. They found that the ordinary kriging and IDW performed very similarly and deemed them to be 'equal'.

Ordinary kriging interpolation tends to smooth out spatial variability and extreme measured values between the range of observed minimum and maximum values for all contaminants. It does not display a true representation of the data (Kazemi and Hosseini, 2011). In their study, Palmer et al. (2009) concluded that kriging techniques in many situations are considered substantially superior compared to IDW techniques as kriging has the quantitative measure of the error associated with each prediction calculated, which is not provided with IDW. IDW interpolation was used in an Osprey egg PCB contamination study conducted by Solla and Martin (2008) because IDW reduces the influence of more distant observations.

Li and Heap (2011) provided a summary of many factors that affect the performance of spatial interpolation methods: sampling density, sample spatial distribution, sample clustering, data variance, surface type, data variance, data normality, quality of secondary information, stratification, and grid size of resolution. Kriging and IDW are two interpolation techniques applied widely to elucidate spatial variation and spatial distribution of many contaminants (Gu et al., 2012; Li and Heap, 2008; Palmer et al., 2009; Xie et al., 2011).

2.3 PCB and PAH Research

Total PCBs and PAHs act differently in aquatic environments (Foster and Cui, 2008). Both PAHs and Total PCBs are generally transported by atmospheric emissions or river drainages and are rapidly absorbed onto sediments and soil particles due to their low aqueous solubility and high octanol-water partition coefficients (Feo et al., 2011; Foster and Cui, 2008). PAHs and PCBs display high unpredictability following release, causing sudden variations of environmental chemical-physical properties (Feo et al., 2011). This causes a concern in the St. Marys River due to the constant shipping traffic and canal dredging. Foster and Cui (2008) found that the molecular composition of PCBs in sediments on a relative basis was not nearly as consistent as that observed for PAHs. PCBs and PAHs tend to not display similar spatial distribution patterns, as sediment concentrations of PCBs do not always have a downstream concentration gradient as seen often with PAHs. PCB emissions tend to rather be more localized around point sources, usually found next to industrial, utility, or waste-site sources (Foster and Cui, 2008).

PCBs showed less overall influence with proximity to urban regions, but rather the highest PCB concentrations were derived from urban structures of some type, such as outfalls or storm sewers, as PCBs are primarily found near point source discharges (Foster and Cui, 2008). For example, Solla and Martin (2008) found that the highest concentration of PCBs was located next to the Lindsay, Ontario sewage lagoons, twice as high than immediately upstream, further away from the urbanization. Other than the group of outliers, the findings agreed with other PCB interpolation studies, that there is a clear relationship between a point source and higher contamination concentrations, and a decline in concentrations from the maximum sediment depths.

Since PAHs are a group of organic compounds, the molecular weight (two or more fused aromatic rings) of contaminants can produce different trends. PAHs show rising concentrations in river sediments closest to an urban environment. In urbanized areas, runoff has been established as a major source of PAHs to the aquatic environment, with particularly high levels derived from industrial discharges and impervious surface runoff. It is important to interpret dispersive population density factors and specific urban structures, such as bridges and point-source outfalls while analyzing downstream concentration profiles (Foster and Cui, 2008). Other contributing PAHs contaminant sources include areas where high levels of human activities occur: residential heating, power generation, recreation and school areas, and vehicle emissions (De La Torre-Roche et al., 2009).

In their study, Feo et al. (2011) found that PAHs are localized in areas dominated by the effects of pyrogenic influences. In contrast, the lowest levels of PAHs tend to be found in samples from sites registered near agricultural and remote areas (De La Torre-Roche et al., 2009). Foster and Cui (2008) conclusions were similar, as they found that trends of PAHs in aquatic sediments of the upper Potomac River, Maryland were correlated with population density and the extent of urban land use, likely through areal dispersal following combustion, along with point sources (bridges and outfalls). Historical trends in PAHs concentrations analyzed from sediment cores from lakes and reservoirs in North America show that the greatest rise of PAHs is occurring in regions of rapid urbanization and sprawl (De La Torre-Roche et al., 2009; Foster and Cui, 2008).

CHAPTER 3: DATA AND METHODOLOGY

3.1 Data

The contamination data were provided by Environment Canada through the Canada Centre for Inland Waters. Data were collected for areas throughout the St. Marys River in a non-uniform pattern on November 2nd, 2010. There were a total of 36 core samples collected, while only 17 core samples will be analyzed in this study at depths of 0-5 cm and 5-10 cm (Figure 3.1). The samples excluded from this study were either located at a location further away from the 17 clustered samples, contained null values in their contaminant information, were located in shallow water, or not located within the primary river basin channel (Figure 3.1). The river depths of the selected sample locations range from 4.3 to 7.5 metres.

The Canada Centre for Inland Waters produced information for 47 different contaminants, however only five contaminants will be used in this study (Total PAHs, Total PCBs, flourene, anthracene, and pyrene). All samples were analyzed using the same methods, and were then frozen and archived. All sample locations for Total PAHs, anthracene, pyrene and flourene contain values at both depths. The Total PCB samples were collected only at depths of 0-10 cm.

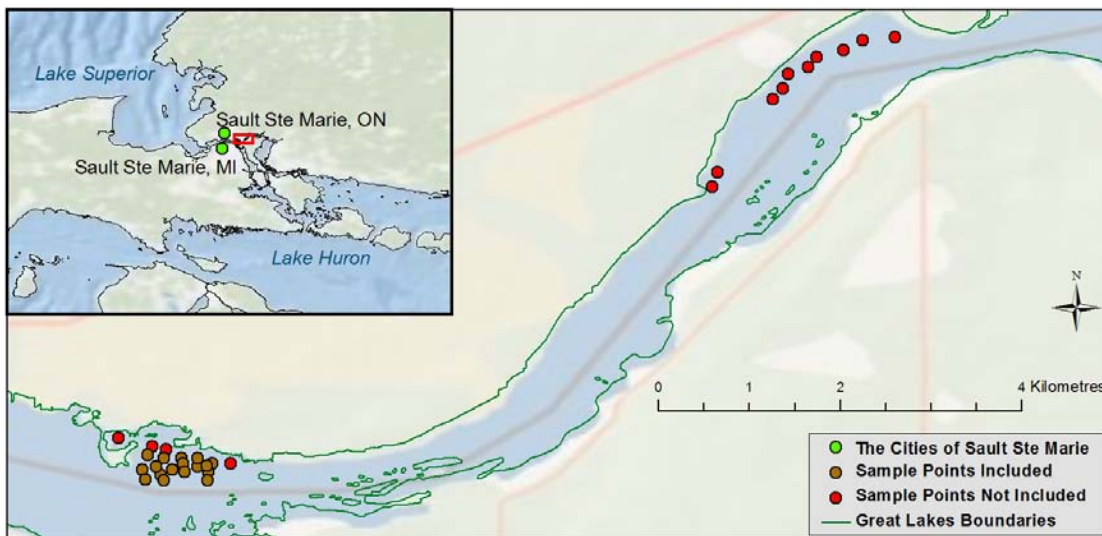


Figure 3.1: Sample point distribution within the study area.

The descriptive statistics for Total PAHs, anthracene, pyrene and flourene can be seen in Table 3.1 (0-5cm) and Table 3.2 (5-10cm). The descriptive statistics for Total PCBs can be seen in Table 3.3. There are 17 samples analyzed at both depths. Several important trends emerge while analyzing the pre-transformed descriptive statistics. Spatial interpolation methods prefer normality in the data, as skewness is a measure of the asymmetry of the probability distribution. The closer the skewness value is to 0, the more indicative of a ‘normal distribution’. The skewness values of all the contaminants in Tables 3.1, 3.2 and 3.3 indicate a non-normal distribution in the data. These values are not ‘ideal’ for the ordinary kriging and IDW techniques. The variance statistic (seen in Tables 3.1, 3.2, and 3.3) is a measure of how far the set of values are spread out, as a smaller variance value is preferred (similar to skewness). The variance values in the Tables are extremely high, not being ideal for IDW and ordinary kriging.

Table 3.1: Contaminant descriptive statistics for depths of 0-5cm. The asterisk (*) denotes that variable has been transformed.

	Range	Min.	Max.	Mean	Std. Deviation	Variance	Skewness
Fluorene	193	121	314	217.76	52.118	2716.29	-0.46
lg10Flourene*	0.41	2.08	2.5	2.3252	0.11044	0.012	-0.37
Anthracene	748	162	910	398.29	169.388	28692.314	1.578
lg10Anthracene*	0.75	2.21	2.96	2.5678	0.16913	0.029	0.272
Pyrene	2990	1240	4230	2297.62	741.828	550309.048	0.718
lg10Pyrene*	0.53	3.09	3.63	3.3401	0.1392	0.019	0.027
Total PAHs	26010	14150	40160	25357.6	8099.508	65602034.9	0.338
lg10PAHs*	0.45	4.15	4.6	4.3825	0.14183	0.02	-0.088

Table 3.2: Contaminant descriptive statistics for depths of 5-10cm. The asterisk (*) denotes that variable has been transformed.

	Range	Min.	Max.	Mean	Std. Deviation	Variance	Skewness
Fluorene	389	232	621	416.29	126.897	16102.914	0.258
lg10Flourene*	0.43	2.37	2.79	2.5995	0.13614	0.019	-0.137
Anthracene	1667	253	1920	865.86	475.021	225645.33	0.812
lg10Anthracene*	0.88	2.4	3.28	2.8753	0.24075	0.058	0.003
Pyrene	7860	2050	9910	4628.1	2163.145	4679196.2	1.037
lg10Pyrene*	0.68	3.31	4	3.6235	0.19325	0.037	0.283
Total PAHs	70879	21389	92268	47425.7	18996.12	360852609	0.584
lg10PAHs*	0.63	4.33	4.97	4.6422	0.17766	0.032	-0.069

Table 3.3: Total PCB descriptive statistics for depths of 0-10cm. The asterisk (*) denotes that variable has been transformed.

	Range	Min.	Max.	Mean	Std. Deviation	Variance	Skewness
TOTAL PCBs	116	8	124	60.33333	31.0360006	963.23	0.304
lg10PCBs*	1.19	0.9031	2.0934	1.707094	0.290056	0.084	-1.221

Several studies have found that contamination concentrations decrease in value with depth (Feo et al., 2011; Heidtke et al., 2006; Sower and Anderson, 2008); however, the descriptive statistics in Tables 3.1 and 3.2 display a different trend for this study area

as the range, minimum, maximum, mean, standard deviation, and variance increase from 0-5cm to 5-10cm depths. The high mean and variance statistics in Table 3.1 indicate that adverse biological effects are likely occurring in the study area. These statistics increase drastically with depth (Table 3.2), causing further biological risk concerns, which become apparent when concentrations exceed the TEL.

A few other trends are important to observe prior to processing the contamination values; the anthracene values are between the TEL and PEL levels at depths of 0-5cm (Table 3.1), but exceed the PEL levels at the 5-10 cm depth (Table 3.2); the minimum values at both depths for flourene and pyrene exceed the PEL levels (Tables 3.1 and 3.2); and the total PAHs are the only contaminant that contains values remaining between the TEL and PEL levels at both depths (Tables 3.1 and 3.2). Total PCBs (Table 3.3) displayed the lowest mean, standard deviation, variance, and skewness statistics out of all contaminants. Even though the values were the lowest, they are still not preferred statistics for ordinary kriging interpolation.

3.2 Methodology

Both ordinary kriging and IDW spatial interpolation techniques were used to assess the subsurface sediment contamination. The individual contamination results were then used to compare the two spatial interpolation techniques through the predicted surface maps and cross validation statistics (see Figure 3.2).

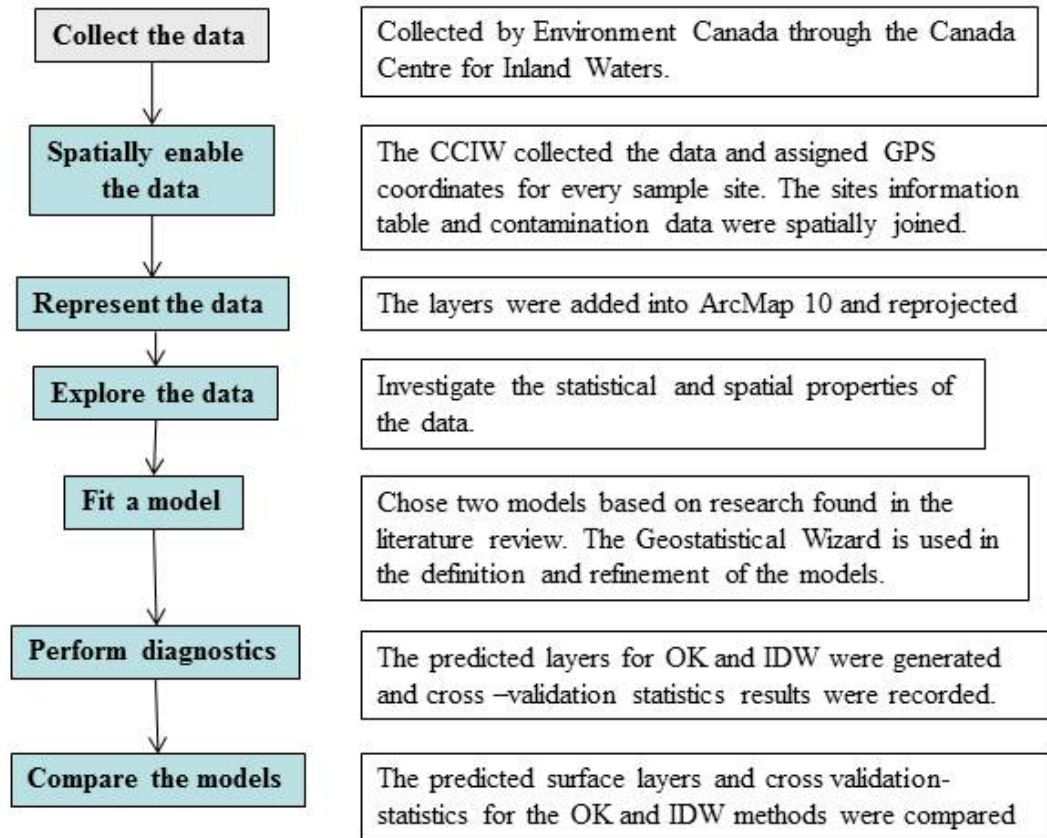


Figure 3.2: Methodology workflow; derived from Johnston et al. (2001).

The kriging technique uses “statistical models that are based on the assumption that spatial autocorrelation exists within a collection of sampled points” (Forsythe et al., 2010; Gawedzki and Forsythe, 2012; Kazemi and Hosseini, 2011; Rodriguez, 2009). IDW is an exact interpolator method based on the assumption that nearby values contribute more to the interpolated values than distant observations. In other words, the degree of influence is expressed as the inverse of the distance between points raised to a power (Joseph et al., 2010; Palmer et al., 2009; Salihoglu et al., 2011).

The kriging interpolation method is considered to have a major advantage over other spatial interpolation methods because it can be statistically validated as it generates

multiple standard error surfaces and cross validation statistics (Forsythe et al., 2010; Gazedzki and Forsythe, 2012; Jakubek and Forsythe, 2004; Johnston et al., 2001). However, the IDW technique provides some cross validation statistics as well, and is considered an exact interpolator (Aelion et al., 2008; Joseph et al., 2010).

The spherical model for ordinary kriging was used as several studies used the spherical model while analyzing the semivariance in ordinary kriging. It was found to be the preferred model as it produces the most ideal error statistics out of all other ordinary kriging models (Gawedzki and Forsythe, 2012; Joseph et al., 2010; Kazemi and Hosseini, 2011; Rodriguez, 2009). The spherical model has a wide applicability when modelling natural phenomena (Clark, 1979).

The criteria to produce the most appropriate parameters for both the ordinary kriging and IDW interpolation methods were chosen after experimentation. The parameters selected produced the most accurate results when compared to other options. ESRI's ArcMap 10.0 Geostatistical Wizard helps to provide automatic parameter calculations assisting users find the most accurate results (Kazemi and Hosseini, 2011). The calculations assisted in producing the parameters in this study. The following parameters were derived for the ordinary kriging method: Maximum Range: 0.00915; Minimum Ranges: 0.003624; Direction: 75; Neighbours to Include: 5; Include at Least: 2; Lag Size: 0.00076; Partial Sill: 0.1307; Nugget: 0.00195.

The maximum and minimum ranges are derived from the distances between the sampling points. Although the sample size in the study area was small (17 sample points), 5 neighbours to include were used because the points are clustered closely together and the higher number could decrease the spatial autocorrelation among

measured points to occur. Include at least 2 neighbours was used due to the small number of sample points (Gawedzki and Forsythe, 2012). The lag size helps reveal any spatial relationships in the data, as a small lag size models local variation between neighbouring points more accurately (Johnston et al., 2001). The spherical model also contains the sill and nugget: sill represents a value where the semi-variance become constant, meaning spatial autocorrelation ceases to be a factor; and nugget represents measurement errors, random errors, or possible small variations undetected by the semivariogram (Johnston et al., 2001; Joseph et al., 2010; Rodriguez, 2009). The anisotropy parameter on the semivariogram dialog box was set to true. Doing this allows the single line in the semvariogram to become many lines, accounting for many directions. The many lines (models) produce a theoretical “best fit” semivariogram model (ESRI, 2010; Johnston et al, 2001).

ESRI’s ArcMap 10.0 Geostatistical Wizard was used for the IDW methodology. The standard neighbourhood type was used, as several studies chose it as the preferred method (Aelion et al., 2008; Gu et al., 2012; Li and Heap, 2011; Xie et al., 2011). The standard option assigns weights based on distance from the target location, as the smooth option adjusts the weights using a sigmoidal (S-shaped) function defined by the smoothing factor (Dille et al., 2002; Palmer et al., 2009; Salihoglu et al., 2011). The standard neighbourhood method uses similar parameters as the ordinary kriging method; therefore, the same values were used: Maximum Neighbours (Neighbours to Include): 5; Minimum Neighbours (Include at Least): 2; Major Semiaxis (Maximum Range): 0.00915; Minor Semiaxis (Minimum Range): 0.003624; Angle (Direction): 75. A power of 1 and an Anisotropy factor of 2.525 were also input. The power function option

allows the user to take control of the influence of known values on the interpolated values, based on their distance from the predicted point. As a result, as the distance increases, the weights decrease rapidly. If the power value is very high, only the immediate surrounding points will become influential in the prediction. The default value for IDW in the Geostatistical Wizard is 2, known as the inverse distance squared weighted interpolated (ESRI, 2010). The optimal value of 1 was determined by experimentation, reducing the cross validation statistics as much as possible. Salihoglu et al. (2011) state that a power of 1.0 indicates a constant rate of change in value between points (i.e., a linear interpolation).

3.3 Cross Validation Statistics

To determine the most appropriate spatial interpolation method, a set of cross-validation error statistics should be compared. Since this study is comparing IDW and ordinary kriging, only the root mean square and mean statistics will be used for comparison, as IDW does not calculate the mean standardized (MS), SRMPSE, and average standard error (ASE) statistics. The cross validation procedure consists of the removal of one sample value from the dataset and the estimation of a value at the very same point with n-1 samples (Joseph et al., 2010; Li and Heap, 2011; Li et al., 2011). The difference between sampled values and estimated values gives an indication of how well the predicted values fit in the neighbourhood of sampled values (Johnston et al., 2001). This allows the two models to be compared on the basis of how well they estimated the measured sample values. The ideal MPE value needs to be as close to 0 as possible and the RMSPE should not be more than 20 (ESRI, 2010; Forsythe et al., 2010).

The MPE is used for determining the degree of bias in estimates and is often simply referred to as the ‘bias’ (Isaaks and Srivastava, 1989; Joseph et al., 2010). It should be used cautiously as an indicator of accuracy only because the negative and positive values counteract each other and the MPE result tends to be lower than the actual error (Li and Heap, 2011). If the MPE is negative, the model has overestimated the real value, as a positive value means the model has underestimated the value (Johnston et al., 2001). The general MPE formula is as follows:

$$ME = \frac{1}{n} \sum_{i=1}^n (p_i - o_i) \quad (3)$$

where n represents the number of observations or samples, o is the observed values, and p is the predicted or estimated values (Li and Heap, 2011).

The RMSPE is an estimate of the global difference between the observed and the estimated surface. A relatively small value for the RMSPE indicates a good global estimation of the interpolated surface in comparison with the original surface. Contrary to MPE, the RMSPE does not provide negative values (Johnston et al., 2001). Although the RMSPE provides a measure of error, it is sensitive to outliers as it places a lot of weight on large errors (Isaaks and Srivastava, 1989; Li and Heap, 2011). The RMSPE also does not provide information on the relative size of the average difference and the nature of differences comprising the data (Joseph et al., 2010). For the nature of this study, the RMSPE is an appropriate cross validation statistic as it is calculated the same way for both ordinary kriging and IDW. Li and Heap (2011) described the RMSPE as one of the best overall measures of model performance because it summarizes the mean difference in the units of observed and predicted value. The general RMSPE formula is as follows:

$$\text{RMSE} = \left[\frac{1}{n} \sum_{i=1}^n (p_i - o_i)^2 \right]^{1/2} \quad (4)$$

where n represents the number of observations or samples, o : observed values, p : predicted or estimated values (Li and Heap, 2011).

The SRMSPE is equal to the square root of the sum of the predicted errors divided by the squared standard deviation divided by the total number of samples (Johnston et al., 2001; Rodriguez, 2009). The ideal value is one, as under or over estimation of the variability of the predicted values occurs if the SRMSPE is greater or lower than one (Johnston *et al.*, 2001).

3.4 Log-Transformations

Most spatial interpolation techniques do not require normality in the data; however, normality is essential for kriging, although it is not necessarily required. Some authors performed transformations to normalize their values, as they argue that non-normal distributions need to be transformed (De La Torre-Roche et al., 2009; Forsythe et al., 2010; Gawedzki and Forsythe, 2012; Gu et al., 2012; Houlding, 2000; Jakubek and Forsythe, 2004; Johnston et al., 2001).

Clark (1979), Gu et al. (2012), and Houlding (2000) found that using a log-normal method for transforming non-normal data works best because the skewness warrants some kind of transformation, as long as no null values exist in the dataset. After the transformation was completed, all variables showed an approximate normal distribution, which significantly reduced the skewness and kurtosis values. In addition, the

transformation helps to make the variance more constant (De La Torre-Roche et al., 2009).

A base ten log function (“LG10()”) was used to standardize the data. Logged values were used for the fitting of theoretical semi-variograms in the ordinary kriging method. Log calculations and transformations were performed in SPSS and the values were used in the ArcGIS Geostatistical Analyst extension (ordinary kriging technique). All the sample points have data available, as there are no null values in the samples. Although IDW does not necessarily require data that has been transformed (to reduce skewness), normalized data was used for consistency. It was also necessary to log transform at both depths to maintain consistency when comparing the results between the depths (Tables 3.4 to 3.9).

Prior to the standardization, the data’s descriptive statistics examined from the samples showed high variance values, maximum, standard deviation, and range values that are not suitable for a spatial interpolation technique (see Tables 3.1 to 3.3). Therefore, the non-normalized data displayed skewness values that were not ideal. Once the log-transformation was performed on the data, the range, maximum, standard deviation, and variance values decreased significantly, resulting in a skewness value becoming ideal for analysis (see Tables 3.1 to 3.3). The ideal skewness value would be 0, which would indicate the perfect distribution, indicating no skewness in the data.

The same trend occurs while examining the MPE and RMSPE values (Tables 3.5 to 3.9). The optimal MPE value needs to be as close to 0 as possible and the RMSPE should not be more than 20 (ESRI, 2010; Forsythe et al., 2010). All but the flourene value at a depth of 0-5cm for both ordinary kriging (Table 3.4) and IDW (Table 3.7), have

MPE values greater than 1.5, which can be improved. When transformed, all the values are closer to zero (being ideal), with the furthest being *lg10Anthracene* at -0.0316 (Table 3.7). The non-transformed RMSPE values follow the same trend, as the lowest RMSPE value is the ordinary kriging Total PCBs (Table 3.6) with a value of 34.19. When transformed, all the RMSPE values are well below the 20 threshold, as the highest value is the ordinary kriging Total PCBs (Table 3.6) with a value of 0.338.

Table 3.4: Contaminant MPE and RMSPE statistics for depths of 0-5cm using ordinary kriging. The asterisk (*) denotes that variable has been transformed.

	MPE	RMSPE
<i>lg10Anthracene*</i>	-0.007262222	0.201989569
<i>Anthracene</i>	-8.477313171	224.0321604
<i>lg10Pyrene*</i>	-0.00317299	0.147670377
<i>Pyrene</i>	-3.591520137	806.3796392
<i>lg10Flourene*</i>	0.003156188	0.121370197
<i>Flourene</i>	1.16975582	55.93543057
<i>lgTotalPAHs*</i>	-0.001416643	0.14352036
<i>Total PAHs</i>	30.35140247	7783.543031

Table 3.5: Contaminant MPE and RMSPE statistics for depths of 5-10cm using ordinary kriging. The asterisk (*) denotes that variable has been transformed.

	MPE	RMSPE
<i>lg10Anthracene*</i>	-0.004762163	0.237758289
<i>Anthracene</i>	-4.88151946	473.7884275
<i>lg10Pyrene*</i>	0.005199288	0.18759761
<i>Pyrene</i>	46.92380218	2120.174545
<i>lg10Flourene*</i>	0.004113605	0.123425518
<i>Flourene</i>	3.541192015	128.4892904
<i>lgTotalPAHs*</i>	0.004135988	0.176758019
<i>Total PAHs</i>	303.3628163	18964.62445

Table 3.6: Total PCBs MPE and RMSPE statistics for depths of 0-10cm using ordinary kriging. The asterisk (*) denotes that variable has been transformed.

	MPE	RMSPE
<i>lg10PCBs*</i>	0.03535543	0.338462296
<i>Total PCBs</i>	2.4696832	34.19765719

Table 3.7: Contaminant MPE and RMSPE statistics for depths of 0-5cm using IDW. The asterisk (*) denotes that variable has been transformed.

	MPE	RMSPE
<i>lg10Anthracene*</i>	-0.031635425	0.21584198
<i>Anthracene</i>	-19.78041578	216.2996568
<i>lg10Pyrene*</i>	-0.023107345	0.148752652
<i>Pyrene</i>	-25.72413762	808.0216067
<i>lg10Flourene*</i>	-0.01465504	0.118428408
<i>Flourene</i>	-0.024080627	56.70462857
<i>lgTotalPAHs*</i>	-0.023574617	0.145946867
<i>Total PAHs</i>	-186.5709067	8039.845515

Table 3.8: Contaminant MPE and RMSPE statistics for depths of 5-10cm using IDW. The asterisk (*) denotes that variable has been transformed.

	MPE	RMSPE
<i>lg10Anthracene*</i>	-0.036822585	0.277003584
<i>Anthracene</i>	-26.20943381	485.0586355
<i>lg10Pyrene*</i>	-0.014830129	0.207603591
<i>Pyrene</i>	-45.24647096	2149.558903
<i>lg10Flourene*</i>	-0.008658285	0.15296129
<i>Flourene</i>	2.58116622	136.7193155
<i>lgTotalPAHs*</i>	-0.016628461	0.19891701
<i>Total PAHs</i>	-318.6501567	19895.16884

Table 3.9: Total PCBs MPE and RMSPE statistics for depths of 0-10cm using IDW. The asterisk (*) denotes that variable has been transformed.

	MPE	RMSPE
<i>lg10PCBs*</i>	0.016857295	0.272572345
<i>Total PCBs</i>	1.561431247	31.28898299

CHAPTER 4: ANALYSIS

The ordinary kriging and IDW prediction map results were classified into three groups, containing three equal classes. The groups were based on the effect level intervals, as there are three equal classes below the TEL, three equal classes between the TEL and PEL, and three above the PEL (based on the intervals between the TEL and PEL). The number of categories varies among the contaminants as some concentrations may fall within only one or two intervals.

The distribution of sample locations between the three chosen concentration class divisions can be seen in Table 4.1. Overall, the study area portion of the river is heavily contaminated with four of the five contaminants.

Table 4.1: Number of Sediment Sampling Locations in Relation to TEL and PEL Categories

# of Sites		<TEL	≥TEL and <PEL	>PEL
<i>Total PCBs</i>				
0-10 cm	17	3	14	0
<i>Anthracene</i>				
0-5 cm	17	0	2	15
5-10 cm	17	0	0	17
<i>Flourene</i>				
0-5 cm	17	0	2	15
5-10 cm	17	0	0	17
<i>Pyrene</i>				
0-5 cm	17	0	0	17
5-10 cm	17	0	0	17
<i>Total PAHs</i>				
0-5 cm	17	0	17	0
5-10 cm	17	0	17	0

At the 0-5 cm depth, the anthracene and flourene sample points both contain only two samples between the TEL and PEL, while the remaining samples are above the PEL. All the sample point concentrations exceed the PEL at the 5-10 cm depth. The pyrene concentrations exceed the PEL at both depths, while the Total PAHs concentrations are between the TEL and PEL at both depths. The Total PCBs concentrations are the only concentrations to have sample points (three) below the TEL, while the remaining 14 are between the TEL and PEL. These are alarming numbers as the PEL is the concentration where more than 50 percent of the adverse biological effects are encountered for organisms that are in direct contact with the sediments (Canadian Council of Ministers of the Environment, 2001; Keller et al., 2011). The concentrations between the TEL and PEL are also concerning as it is identified as the PER, where 25 percent of the adverse effects persist (Rodriguez, 2009). The drastic changes between depth can be attributed to the chemical compositions of the contaminants as they bind with sediments, and/or the constant shipping traffic, dredging, and storm water runoff occurring in the river (De La Torre-Roche, 2009; Feo et al., 2011; Foster and Cui, 2008; Gawedzki and Forsythe, 2012).

An important note to consider is that Table 4.1 classifies the concentrations based on categories, as it does not show exact sediment core concentrations (Gawedzki and Forsythe, 2012). For example, the two sites in the below TEL class may have values close to the TEL guideline. The values may be near the thresholds, which can still be a cause for concern. Both spatial interpolation methods help provide more detailed surface maps than proportional symbol maps could, as the surfaces clearly display the values in all areas.

4.1 Total PCBs

Figure 4.1.1 displays the sample locations and proportional circle contamination levels for the Total PCBs data at a depth of 0-10 cm. There are only three sample points below the TEL (less than 34.1 ng/g), while the remaining points are all between the TEL and PEL levels (34.1 to 277 ng/g). The three points below the TEL are located in the eastern portion of the study area, surrounded by samples with higher concentrations. There are no concentrations above the PEL (277 ng/g). There appears to be little uniform pattern or consistency of the sample point concentrations.

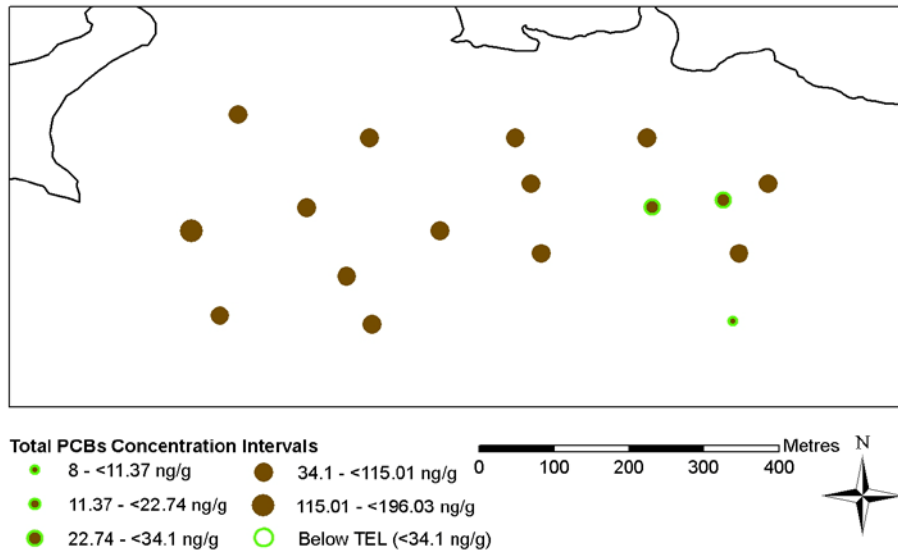


Figure 4.1.1: Distribution of Total PCBs sample point concentrations within the study area at a depth of 0-10 cm.

The ordinary kriging result for sediment contamination of the log-transformed Total PCBs data at a depth of 0-10 cm is depicted in Figure 4.1.2. The majority of the study area appears to be contaminated between the TEL and PEL levels. The highest Total PCBs concentrations are located in the western most portion of the study area.

There are two TEL isolines located in the eastern portion of the study area, as the lowest concentrations are in the south eastern most portions. One of the isolines is in an isolated area surrounded by concentrations between the TEL and PEL. The lowest levels are located in the deepest portions of the St. Marys River. The highest concentrations are located near Topsail Island and in the direction of Sault Ste. Marie.

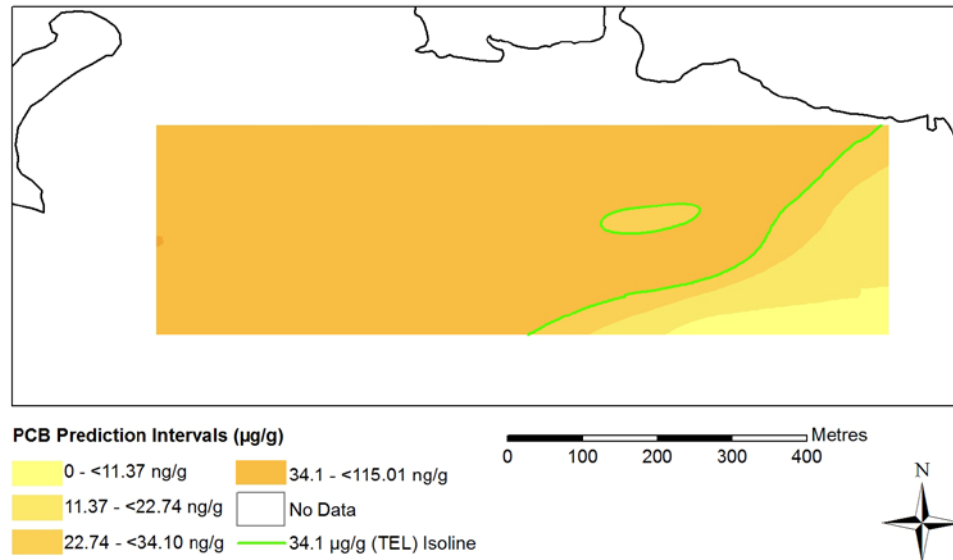


Figure 4.1.2: Ordinary kriging Total PCBs log-normal concentrations at a depth of 0-10 cm.

The IDW results for sediment contamination of the log-transformed Total PCBs data at a depth of 0-10 cm is depicted in Figure 4.1.3. The IDW and ordinary kriging prediction maps display very similar distribution trends. The IDW displays the same heavy concentration in the west, and low concentrations in the south east portion of the study area. The main differences are seen through the ‘bulls-eye’ formations around sample points. IDW produces an additional isoline, dividing up the one isolated area seen

in the ordinary kriging map. The category surface area and boundary characteristics differ from the ordinary kriging map, as there is more variation between classes.

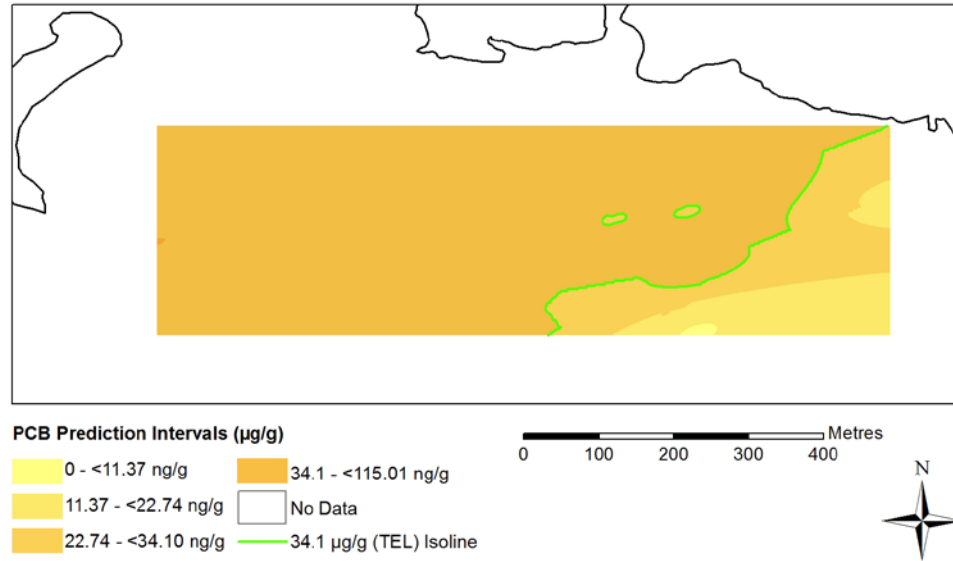


Figure 4.1.3: IDW Total PCBs log-normal concentrations at a depth of 0-10 cm.

The ordinary kriging SRMSPE statistic for Total PCBs is 1.5084, indicating an under estimation of the variability of predicted values. The MPE vales are lower for IDW (0.0168) than ordinary kriging (0.0353) and they both underestimate the real values. IDW has a lower RMSPE (0.2725) than the ordinary kriging (0.3384) and indicates a good global estimation of the interpolated surfaces.

4.2 Anthracene

The majority of the sample sites represented through proportional circles are contaminated above the PEL (>245 ng/g) at the 0-5 cm depth (Figure 4.2.1 (A)). There are only two sample points with concentrations between the TEL and PEL (46.9 to 245

ng/g), which are located in the middle of the study area, surrounded by higher concentration values. There are no concentrations below the TEL.

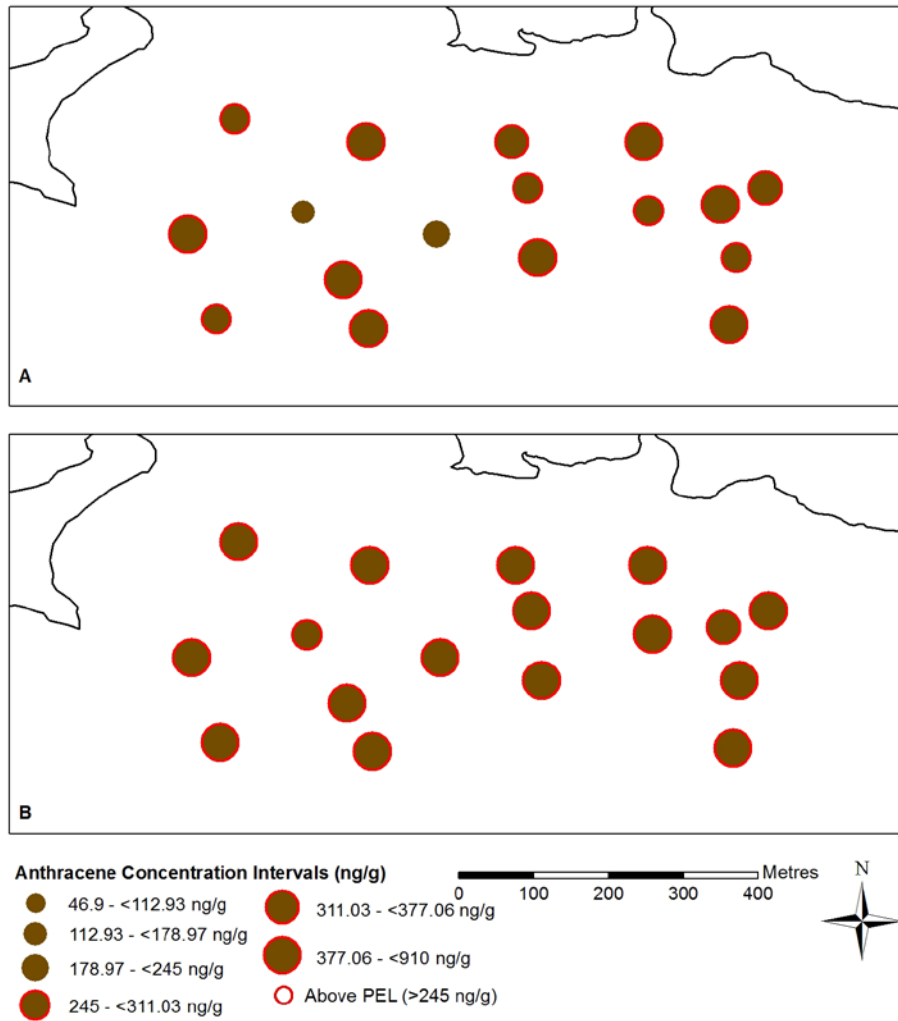


Figure 4.2.1: Distribution of anthracene sample point concentrations within the study area. (A) displays samples at 0-5cm depths and (B) displays samples at 5-10cm depths.

Variation in contamination concentrations between sample points is difficult to identify, as the majority of points fall within the same class. Figure 4.2.1 (B) shows the contamination levels for anthracene at 5-10 cm depth. This layer of sediment is located

directly underneath the 0-5 cm layer, taken from the same core sample. All the concentration points are above the PEL (>245 ng/g). The concentration levels increase drastically at this depth.

The ordinary kriging results for sediment contamination of the log-transformed anthracene data at depths of 0-5 cm (A) and 5-10 cm (B) are depicted in Figure 4.2.2. The ordinary kriging prediction map displays two classes at a depth of 0-5 cm despite variation existing among the sample point concentrations in Figure 4.2.1(A). The minimum range statistics (Table 3.1) and sample point concentration map (Figure 4.2.1A) identify sample points that are below the TEL. The prediction map displays no isolines, as the surface classes are between the TEL and PEL. The 5-10 cm (4.2.2B) prediction map displays a single class throughout the study area. The results at both depths indicate surfaces that have concentrations that exceed the PEL only.

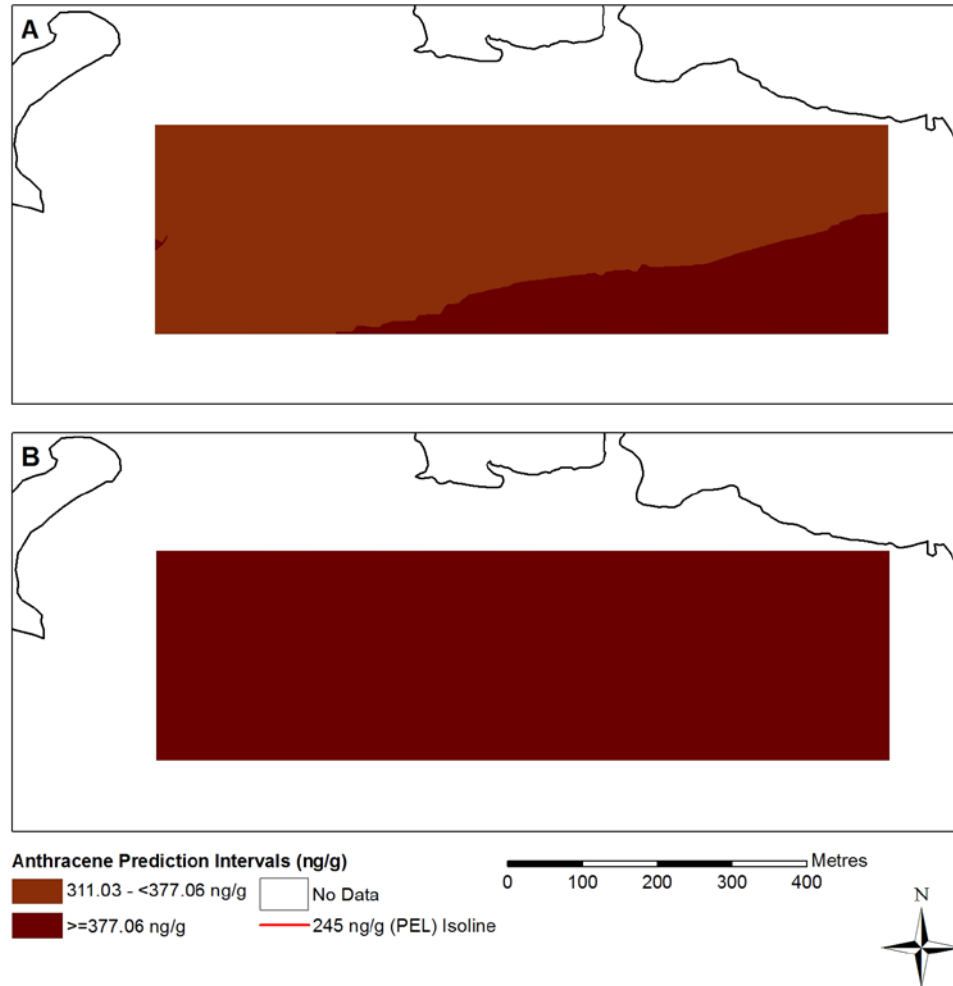


Figure 4.2.2: Ordinary kriging anthracene log-normal concentrations within the study area. (A) displays samples at 0-5cm depths and (B) displays samples at 5-10cm depths.

The IDW results for sediment contamination of the log-transformed anthracene data at depths of 0-5 cm (A) and 5-10 cm (B) are depicted in Figure 4.2.3. The IDW predicted surface maps look considerably different than the ordinary kriging maps, as variation between classes is seen. Although they are small, three PEL isolines are seen in Figure 4.2.3A.

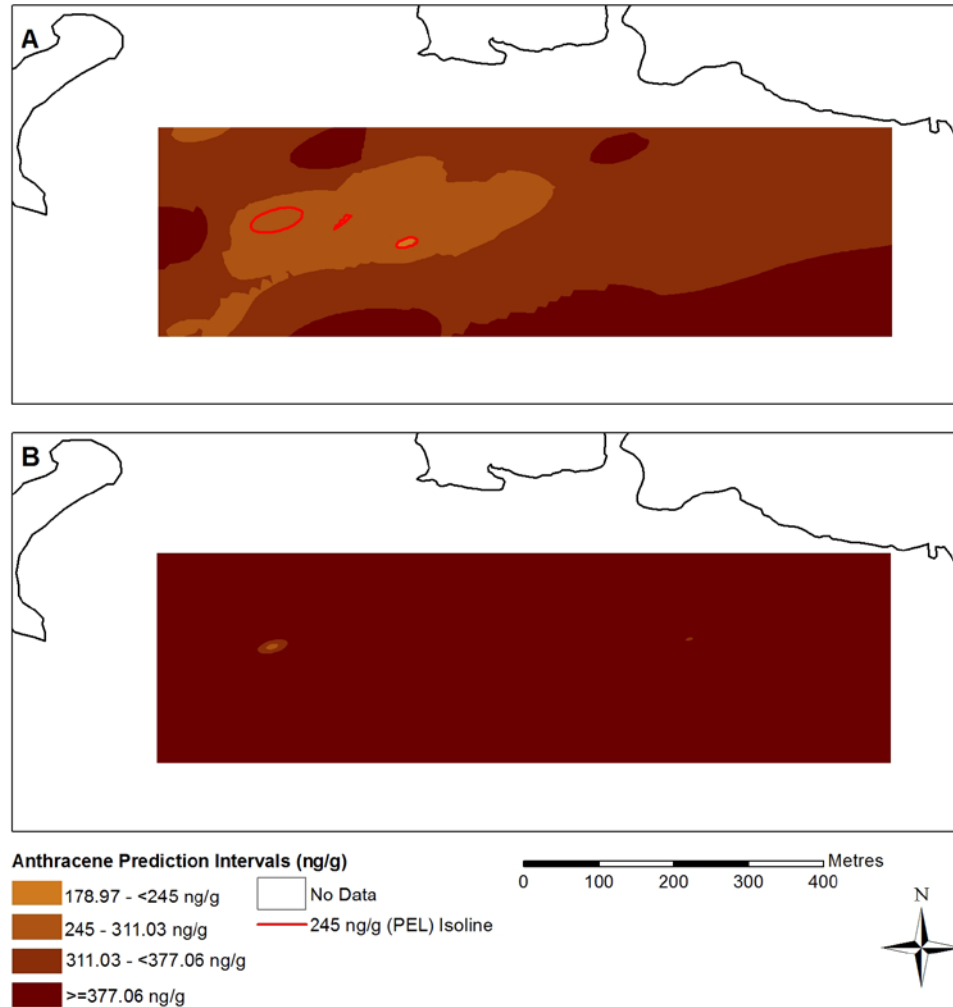


Figure 4.2.3: IDW anthracene log-normal concentrations within the study area. (A) Displays samples at 0-5cm depths and (B) displays samples at 5-10cm depths.

The pockets are located on the western side of the study area, completely surrounded by concentrations exceeding the PEL. There are a total of four different classes represented at the 0-5 cm depth. Higher concentration levels are visible throughout the study area at the 0-5 cm depth, as ‘bulls-eyes’ are formed. There is also a large isolated section of lower concentration levels present in the central portion of the

study area (Figure 4.2.3A). There are three classes in a ‘bulls-eye’ formation represented at the 5-10 cm depth. The remainder of the study area is represented in the highest class.

The ordinary kriging SRMSPE value for the anthracene contamination at the 0-5 cm depth is 1.135, indicating an underestimation of the predicted values. The ordinary kriging (0.2019) and IDW (0.2158) RMSPE values are very similar, as both methods had a good global estimation of the predicted surface (close to 0) in comparison with the original point data. Ordinary kriging’s MPE (-0.0076) is more significant than IDW (-0.0316) as it is closer to 0. The negative MPE values are an overestimation of the real values.

The SRMSPE value for the anthracene contamination at the 5-10 cm depth is 1.0088, indicating a very minor underestimation of the variability. The RMSPE and MPE statistics at the 5-10 cm depth display similar trends to the 0-5 cm depth, as the ordinary kriging RMSPE (0.2377) is lower than IDW (2.77), and the ordinary kriging MPE (-0.0047) is lower than IDW (-0.03682).

4.3 Flourene

Figure 4.3.1 shows the sample locations and proportional circle contamination levels for flourene at depths of 0-5 cm (A) and 5-10 cm (B). The sample point concentrations at both depths follow similar trends as the anthracene data. There are only two points that fall between the TEL and PEL range (21.2 to 144 ng/g) as the remaining points exceed the PEL (>144 ng/g) at the 0-5 cm depth. There is little variation among sample point concentrations at the 0-5 cm depth. The sample point concentrations

increase at 5-10 cm depths, as all the points exceed the PEL (>144 ng/g). More concentration variation exists among the same points at the lower depth.

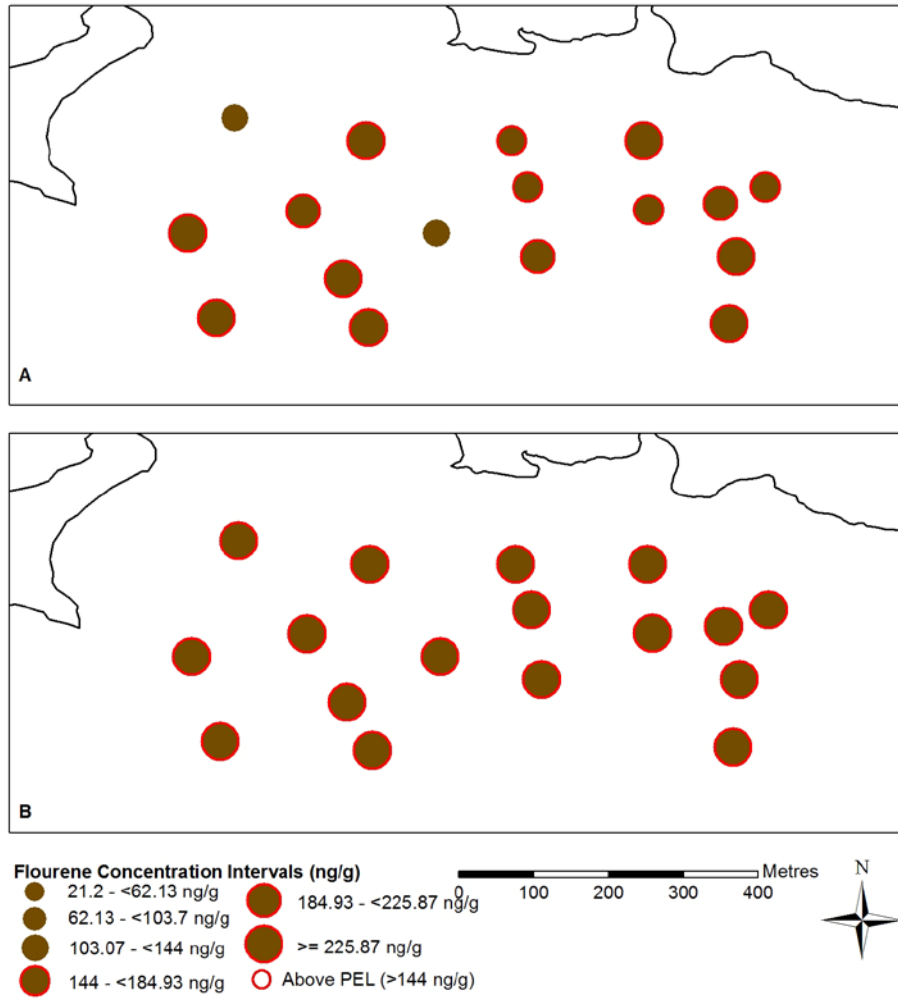


Figure 4.3.1: Distribution of flourene sample point concentrations within the study area. (A) displays samples at 0-5cm depths and (B) displays samples at 5-10cm depths.

The ordinary kriging results for sediment contamination of the log-transformed flourene data at depths of 0-5 cm (A) and 5-10 cm (B) are depicted in Figure 4.3.2. There are three classes represented at the 0-5 cm depth, all above the PEL (4.3.2A). The highest

concentration class is present in the south, as the lower concentrations above the PEL are located in the centre and north western portions of the study area.

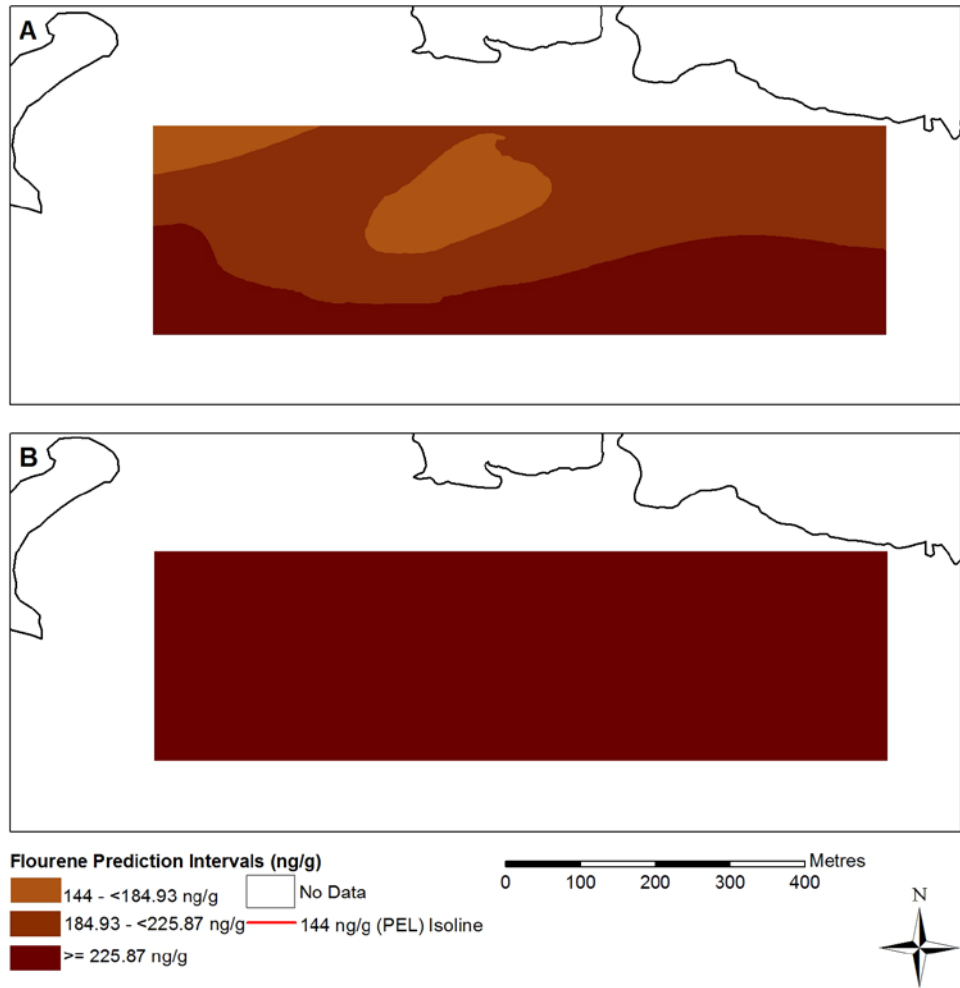


Figure 4.3.2: Ordinary kriging flourene log-normal concentrations within the study area. (A) displays samples at 0-5cm depths and (B) displays samples at 5-10cm depths.

No isolines were identified as all the surfaces produced exceed the PEL values. The concentrations increased in the 5-10 cm depth, as little variation exists in the

prediction surfaces (Figure 4.3.2B). The entire study area is represented by the highest concentration class (≥ 225.87 ng/g).

The IDW results for sediment contamination of the log-transformed flourene data at depths of 0-5 cm (A) and 5-10 cm (B) are depicted in Figure 4.3.3. The IDW results display more variation between classes at the 0-5 cm depth. Similarly to the ordinary kriging result, there is one class dominating most of the study area at the 5-10 cm depth.

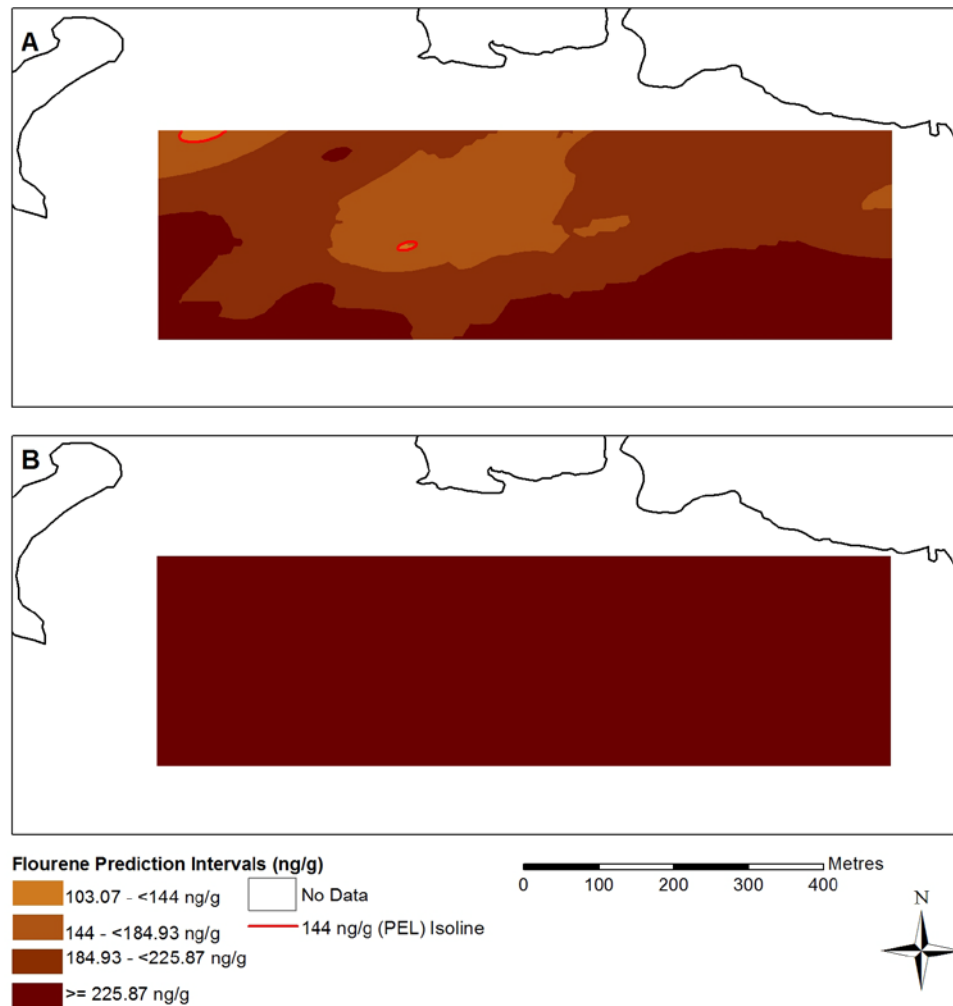


Figure 4.3.3: IDW flourene log-normal concentrations within the study area. (A) displays samples at 0-5cm depths and (B) displays samples at 5-10cm depths.

Unlike the ordinary kriging result, the IDW maps identify two small areas that are between the TEL and PEL (21.2 to 144 ng/g). The smallest isoline area is located in the centre of the study area, completely surrounded by higher concentrations. The other isoline area is located in the north western portion of the study area, near Topsail Island. Multiple 'hotspot' areas are identified throughout the map that are larger, more unified areas at the 0-5 cm depth (Figure 4.3.3A). The large high concentration areas are located in the southern and western portions of the study area. No isolines are present due to all of the values exceeding the PEL.

The ordinary kriging flourene SRMSPE value at the 0-5 cm depth is 1.0893, indicating a minor underestimation of variability of predicted values. The 5-10 cm depth indicates the same (1.03757). The MPE and RMSPE statistics vary significantly between methods. The MPE values at the 0-5 cm and 5-10 cm depths for ordinary kriging are 0.0031 and 0.0041, as they are -0.0146 and -0.0086 for IDW respectively. The ordinary kriging RMSPE values are similar at both depths, while there is a small difference between the IDW values (Tables 3.4, 3.5, 3.7, 3.8). The values are very similar at the 0-5 cm (difference of 0.0028) and 5-10 cm depths (difference of 0.028). All the RMSPE values are below 1.5296, meaning a small difference exists between the observed and estimated surfaces.

4.4 Pyrene

Figure 4.4.1 shows the sample locations and proportional circle contamination levels for pyrene data at depths of 0-5 cm (A) and 5-10 cm (B). The minimum ranges at both depths exceed the PEL (>875 ng/g). There is little variation among the sample point

concentrations at the 0-5 cm depth. The concentrations increase in some sample points at the 5-10 cm depth.

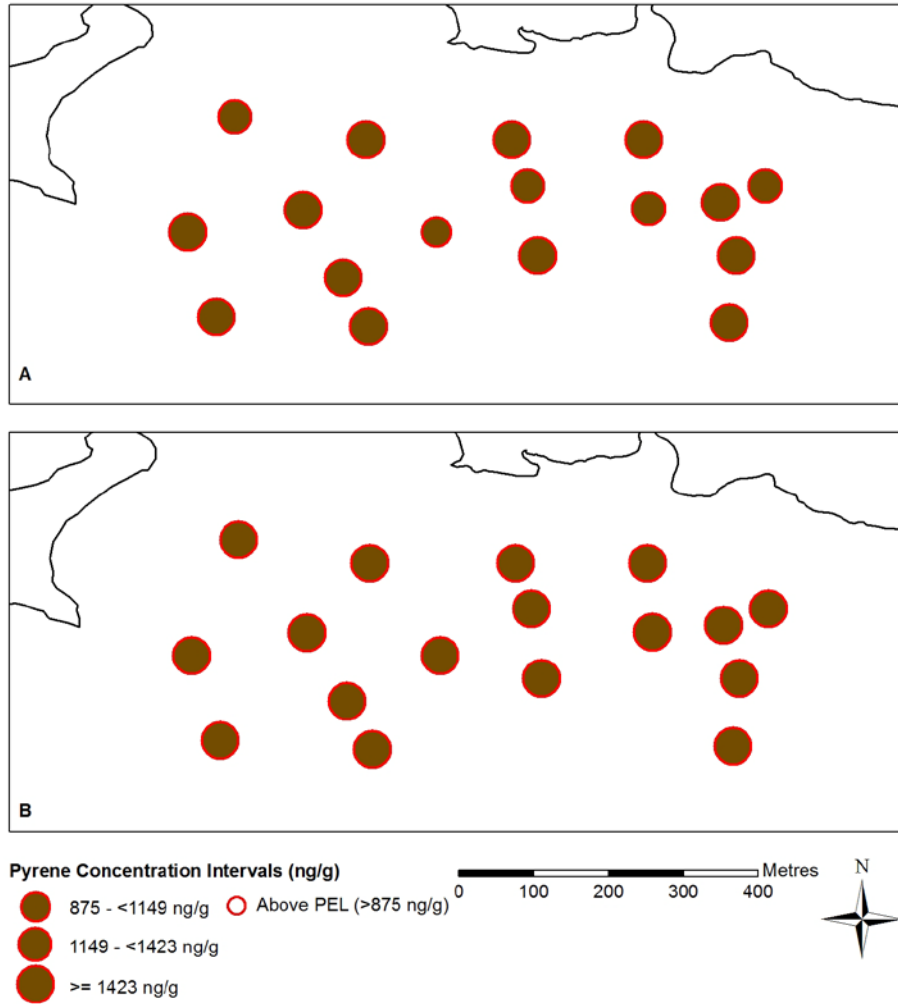


Figure 4.4.1: Distribution of pyrene sample point concentrations within the study area. (A) displays samples at 0-5cm depths and (B) displays samples at 5-10cm depths.

The ordinary kriging results for sediment contamination of the log-transformed pyrene data at depths of 0-5 cm (A) and 5-10 cm (B) are depicted in Figure 4.4.2. The 0-5 cm and 5-10 cm prediction maps display only one class due to the low variation. Both depths display the same single class, even though little variation in the sample point

classes exist. There are no isolines, as all the sample point concentrations exceed the PEL.

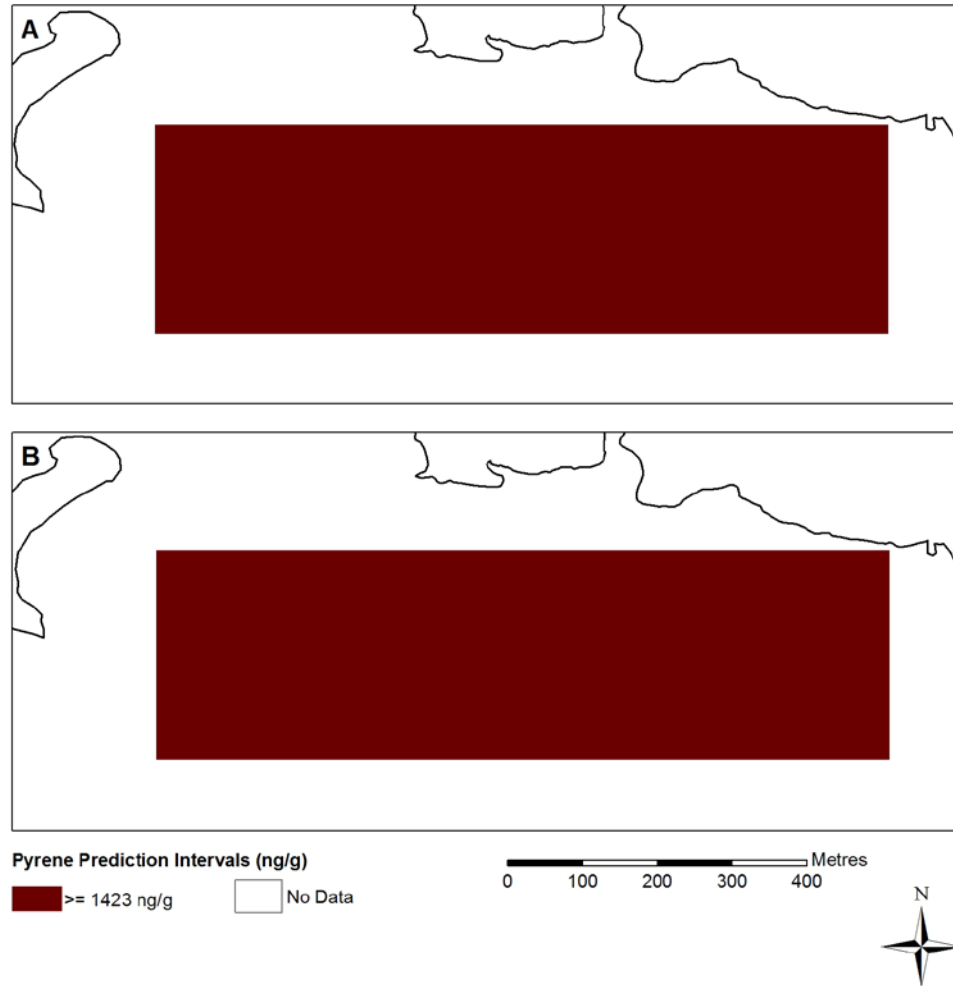


Figure 4.4.2: Ordinary kriging pyrene log-normal concentrations within the study area. (A) displays samples at 0-5cm depths and (B) displays samples at 5-10cm depths.

The IDW results for sediment contamination of the log-transformed pyrene data at depths of 0-5 cm (A) and 5-10 cm (B) are depicted in Figure 4.4.3. The IDW results differ from the ordinary kriging results at the 0-5 cm depth. The 5-10 cm depth displays the same distribution as the ordinary kriging 5-10 cm prediction map (4.4.2B).

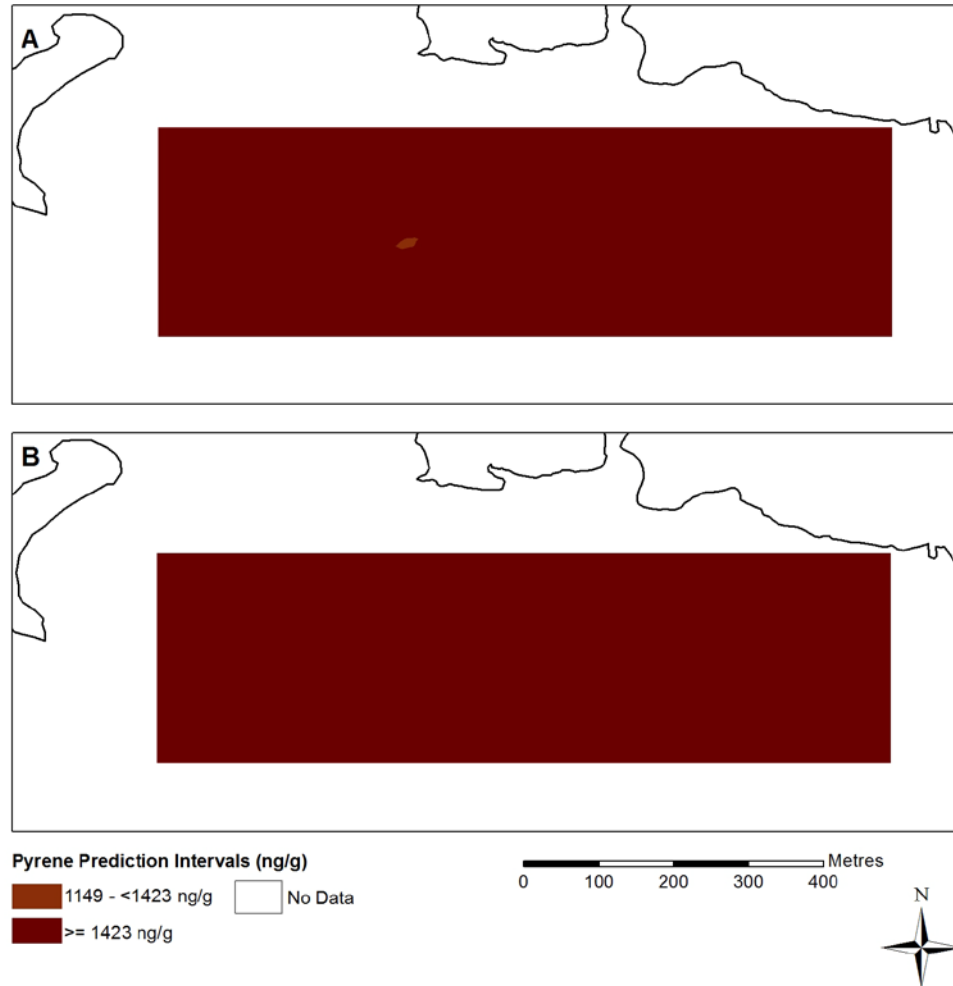


Figure 4.4.3: IDW pyrene log-normal concentrations within the study area. (A) displays samples at 0-5cm depths and (B) displays samples at 5-10cm depths.

There is a 'bullseye' of the lower concentration located in the central portion of the study area for the IDW 0-5 cm depth (Figure 4.4.3A). The highest concentration class dominates the prediction maps at both depths. No isolines are present as all the concentrations exceed the PEL.

The SRMSPE values at both depths (1.0335 and 1.0634 respectively) indicate a small underestimation of variability for the ordinary kriging results. The pyrene MPE values vary significantly at depths and between methods. The RMSPE statistics between IDW and ordinary kriging at both depths are very similar, and indicate a good global estimation.

4.5 Total PAHs

Figure 4.5.1 shows the sample locations and proportional circle contamination levels for Total PAHs data at depths of 0-5 cm (A) and 5-10 cm (B). All of the sample concentrations are between the TEL and PEL (4,000 to 200,000 ng/g) for both depths. There is minimal variation in the data at the 0-5 cm depth (Figure 17A). Many of the sample point concentrations increase at the 5-10 cm depth (Figure 4.5.1B).

There is limited concentration change between depths. The most western sample point displayed the biggest concentration rise, causing a small increase in variation for that portion of the study area.

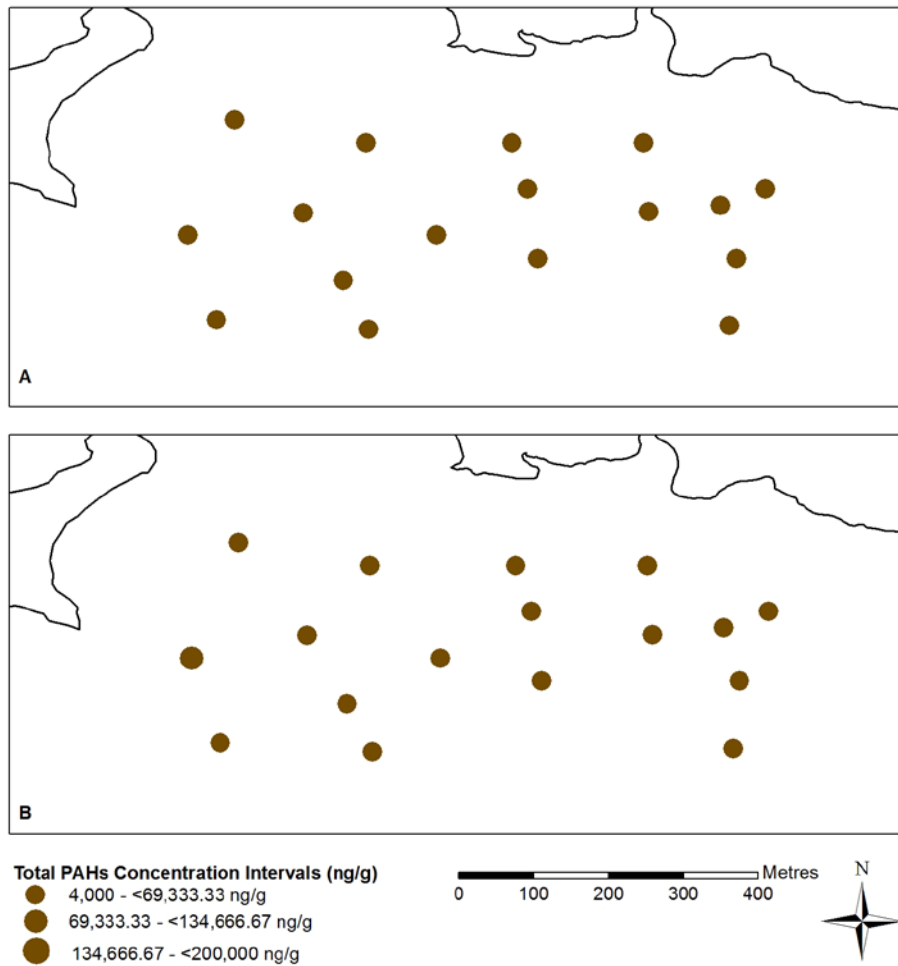


Figure 4.5.1: Distribution of Total PAHs sample point concentrations within the study area. (A) displays samples at 0-5cm depths and (B) displays samples at 5-10cm depths.

The ordinary kriging results for sediment contamination of the log-transformed Total PAHs data at depths of 0-5 cm (A) and 5-10 cm (B) are depicted in Figure 4.5.2. The 0-5 cm and 5-10 cm prediction maps produced a uniform pattern of concentrations as the study areas displayed a single class (4,000 to 69,333.33 ng/g). The entire study area falls within the middle range. Although variation does exist in the data, it is not

represented in the prediction maps. No isolines exist as all the concentrations are between the TEL and PEL.

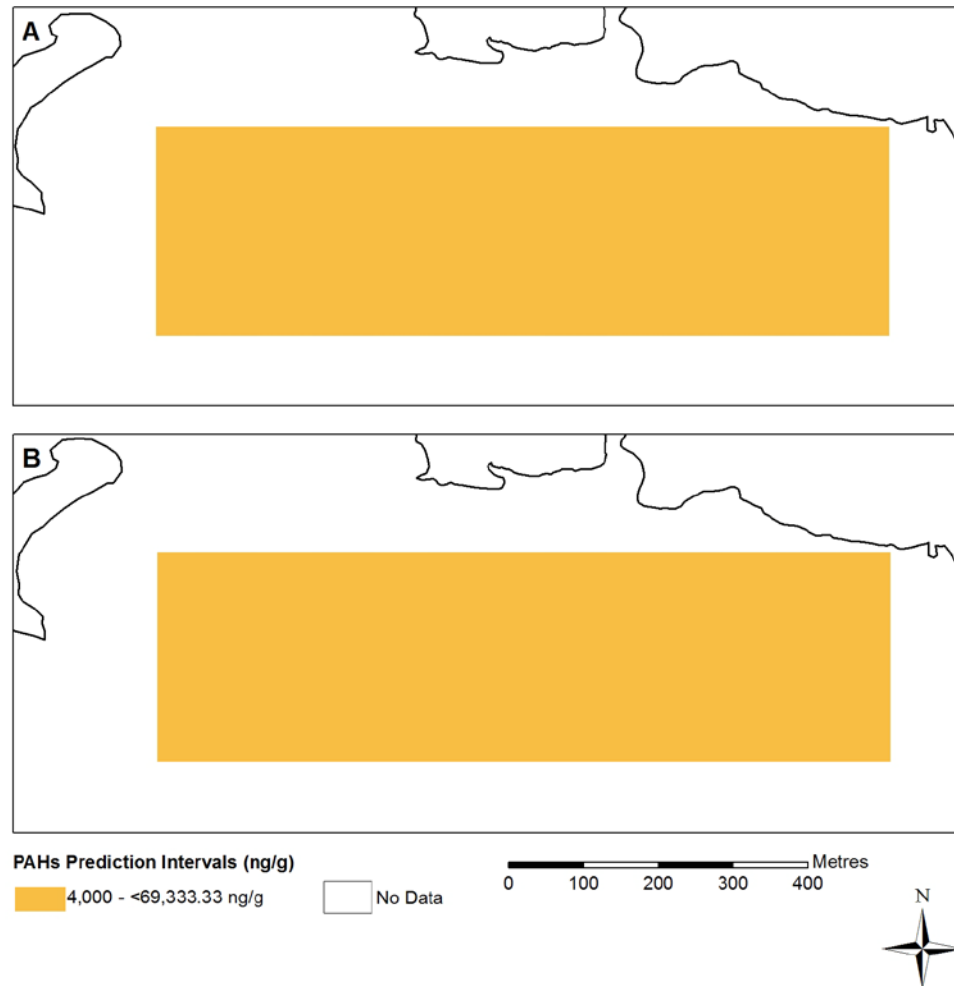


Figure 4.5.2: Ordinary kriging Total PAHs log-normal concentrations within the study area. (A) displays samples at 0-5cm depths and (B) displays samples at 5-10cm depths.

The IDW results for sediment contamination of the log-transformed Total PAHs data at depths of 0-5 cm (A) and 5-10 cm (B) are depicted in Figure 4.5.3. Very little variation exists at the 0-5 cm depth, as a single class is displayed. There is a

concentration ‘bulls-eye’ located in the western part the study area, with only two classes present.

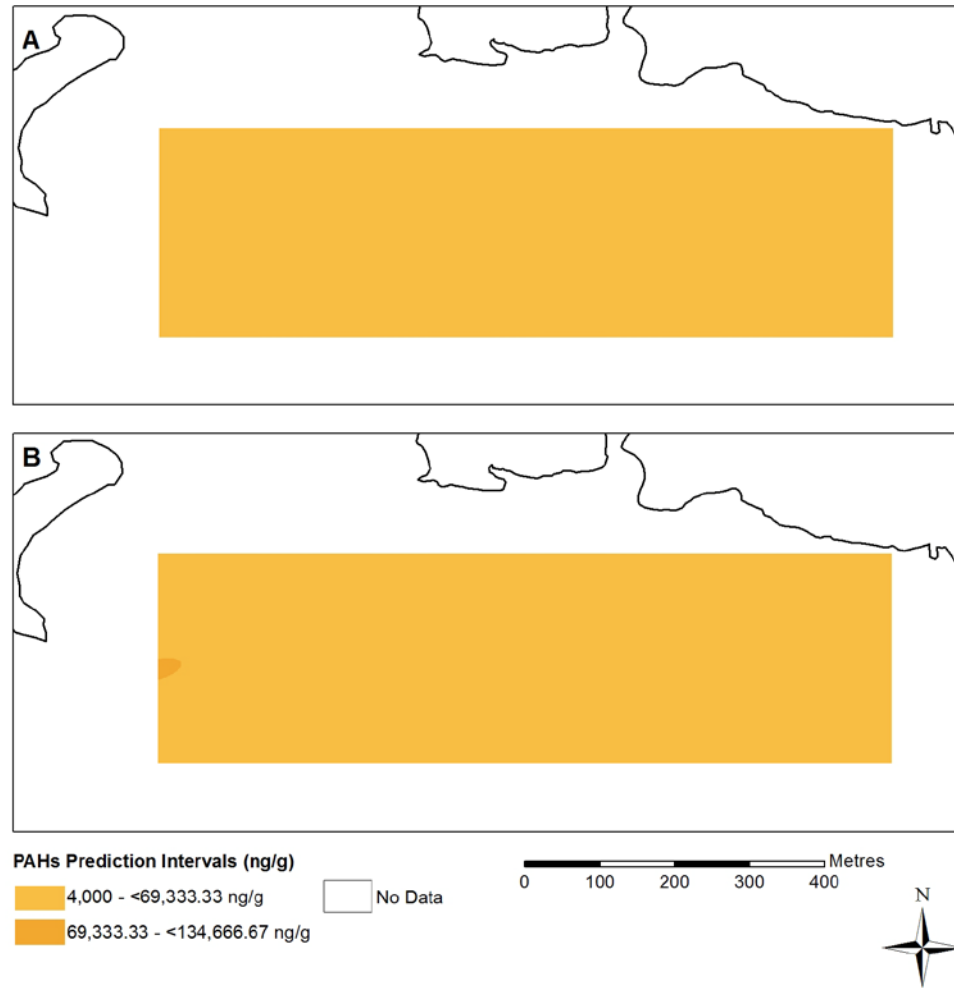


Figure 4.5.3: IDW Total PAHs log-normal concentrations within the study area. (A) displays samples at 0-5cm depths and (B) displays samples at 5-10cm depths.

The ordinary kriging SRMSPE value for the 0-5 cm depth is 0.9851, indicating an overestimation of the variability of predicted values. The SRMSPE value at the 5-10 cm

depth is 1.0729, indicating an underestimation of variability. The RMSPE values for both methods are very similar and they all display a good global estimation of the interpolated surfaces. The MPE values vary between depths for ordinary kriging.

CHAPTER 5: CONCLUSIONS

Water quality began to improve in the St. Marys River and throughout the Great Lakes following the implementation of new environmental regulations in the 1970s and 1980s. The Great Lakes Water Quality Agreement of 1978 was first of many negotiated agreements between Canada and the US. Other important environmental regulations include the Clean Water Act of 1972 and the Canadian Fisheries Act of 1985 (GLWQA, 1978; Ripley et al., 2011). The Remedial Action Plan (RAP) process began in 1988 under the auspices of the Great Lakes Commission as empowered by the Great Lakes Water Quality Agreement (GLWQA, 1987; RAP, 2002). Environment Canada and the Ontario Ministry of the Environment were appointed as the lead agencies for the St. Marys River RAP. Listing of the St. Marys River as an AOC was based on impairments to beneficial uses (GLWQA, 1987; Ripley et al., 2011).

The study area within the St. Marys River is heavily contaminated with anthracene, flourene, pyrene, Total PAHs, and Total PCBs. Areas with contamination concentrations below the TEL pose low risk biological effects, while any areas above the TEL are indicators of ecosystem threats. The most concerning areas are identified above the PEL, as they require the most attention due to the highest chance of adverse biological effects to the ecosystem.

This research was completed to determine which spatial interpolation technique would be most appropriate when examining a small study area with multiple contaminant concentrations. The ordinary kriging and IDW spatial interpolation methods were used to map anthracene, flourene, pyrene, Total PAHs, and Total PCB that are of concern.

Analyzing Total PCB, three PAHs and Total PAHs presented a good measure and the variance of the contamination in the study area.

Although the same data were used, the ordinary kriging and IDW prediction maps display different concentration trends. Depending on the nature of the study, researchers must determine whether they are examining the concentrations locally or globally. Since ordinary kriging is not an exact interpolator, many measured sample values were not represented by their actual values; For example, Figure 4.4.2A displays a single prediction interval class, even though there should be at least two present based on the distribution points (Figure 4.4.1A). The IDW maps display all the variability in the study area through ‘hot’ and ‘cold spots’; for example, Figure 4.3.3A displays three classes with many small hot and cold spots identified. In this study, the IDW maps may provide more insight to point source contamination and reasons for variation than the ordinary kriging maps.

Both the IDW and ordinary kriging spatial interpolation techniques have drawbacks. The maximum calculated value with ordinary kriging was lower than some of the measured sample values because ordinary kriging is not an exact interpolator and the surface generated is a function of spatial relationships among the measured values. IDW is an exact interpolator, but the prediction error was higher and the interpolated surfaces created ‘bulls-eyes’ around the samples (Joseph et al., 2010).

5.1 Recommendations and Further Research

More samples need to be obtained that incorporate the entire river, as a small sample sizes will only create a very focused snapshot (Sower and Anderson, 2008). The greater the observation density, the better the predictions (Palmer et al., 2009). With more sample points, a direct source can be determined. Essentially, the contaminants could 'point' to the contributor.

There was little variation amongst classes in most of the contaminants; however, the classes sometimes had extremely large ranges. By increasing the number of classes and reducing the class ranges, much more variation may be observed. This could help solve problems of having an excess amount of classes that might not lead to consistency when mapping multiple concentrations.

REFERENCES

- Aelion, C. J., Davis, H. T., McDermott, S., and Lawson, A. B. 2008. Metal Contaminations in rural topsoil in South Carolina: Potential for human health impact. *Science of the Total Environment*, 402, 149-156.
- Arbic, B., 2003. City of the Rapids: Sault Ste. Marie's Heritage. *Priscilla Press, Allegan, Michigan*.
- Breivik, K., Sweetman, A., Pacyna, J., and Jones, K. 2002. Towards a global historical emission inventory for selected PCB congeners – a mass balance approach 2. *Science of the Total Environment*, 290, 199-224.
- Canadian Council of Ministers of the Environment. 1999. Canadian Environmental Quality Guidelines. *Winnipeg, MB, Canada*.
- Childs, C. 2004. Interpolating Surfaces in ArcGIS Spatial Analyst. *ArcUser*, July, 32-35.
- Clark, I. 1979. Practical Geostatistics. *Essex: Applied Science Publishers*.
- De La Torre-Roche, R. J., Lee, W.-Y., and Campos-Diaz, S. I. 2009. Soil-borne polycyclic aromatic hydrocarbons in El Paso, Texas: Analysis of a potential problem in the United States/Mexico border region. *Journal of Hazardous Materials*, 163, 946-958.
- Dille, J. A., Milner, M., Groeteke, J. J., Mortensen, D. A., and Williams II, M. M. 2002. How good is your weed map? A comparison of spatial interpolators. *Weed Science*, 51, 44-55.
- ESRI, Inc. 2010. ArcGIS 10 Help. *Redlands, California*.
- Feo, M. L., Sprovieri, M., Gherardi, S., Sammartino, S., and Marsella, E. 2011. Polycyclic aromatic hydrocarbons and polychlorinated biphenyls in the harbour of Naples (Southern Italy): time and spatial distribution patterns. *Environmental Monitoring and Assessment*, 174, 445-459.
- Forsythe, K.W., Gawedzki, A., and Rodriguez, P.S. 2010. Assessing Sediment Contamination in the Buffalo River. In: *Strobl, J., T. Blaschke, and G. Griesebner (Eds.) Proceedings of the 22nd Symposium for Applied Geographic Information Processing (Angewandte Geographische Informationsverarbeitung XXII), AGIT 2010. July 7-9, 2010. Salzburg, AUSTRIA. Herbert Wichmann Verlag, Hüthig GmbH and Co. KG, Heidelberg, Germany. pp. 606-615.*
- Forsythe, K. W., and Marvin, C. H. 2009. Assessing historical versus contemporary mercury and lead contamination in Lake Huron sediments. *Aquatic Ecosystem Health and Management*, 12(1), 101-109.

- Forsythe, K. W., and Marvin, C. H. 2005. Analyzing the spatial distribution of sediment contamination in the lower Great Lakes. *Water Quality Research Journal of Canada*, 40(4), 389-401.
- Foster, G. D., and Cui, V. 2008. PAHs and PCBs deposited in surficial sediments along a rural to urban transect in a Mid-Atlantic coastal river basin (USA). *Journal of Environmental Science and Health Part A*, 43, 1333-1345.
- Gawedzki, A. and Forsythe, K. W. 2012. Assessing Anthracene and Arsenic Contamination within Buffalo River Sediments. *International Journal of Ecology Article ID 496740*, 9 pages, doi:10.1155/2012/496740
- Gu, Y.-G., Wang, Z.-H., Lu, S.-H., Jiang, S.-J., Mu, D.-H., and Shu, Y.-H. 2012. Multivariate statistical and GIS-based approach to identify source of anthropogenic impacts on metallic elements in sediments from the mid Guangdong coasts, China. *Environmental Pollution*, 163, 248-255.
- Great Lakes Water Quality Agreement (GLWQA) of 1978, as amended by Protocol on November 18, 1987. *International Joint Commission, United States and Canada*.
- Heidtke, T., Hartig, J. H., Zarull, M. A., and Yu, B. 2006. PCB Levels and Trends within the Detroit River-Western Lake Erie Basin: A Historical Perspective of Ecosystem Monitoring. *Environmental Monitoring and Assessment*, 112, 23-33.
- Houlding, S.H. 2000. Practical Geostatistics - Modeling and Spatial Analysis. *Berlin: Springer*.
- Isaaks, E. H., and Srivastava, R. M. 1989. An Introduction to Applied Geostatistics. *New York: Oxford University Press*, 249-266 & 278-322.
- Jakubek, D. J., and Forsythe, K. W. 2004. A GIS-based kriging approach for assessing Lake Ontario sediment contamination. *Great Lakes Geographer*, 11(1), 1-14.
- Johnston, K., VerHoef, J.M., Krivoruchko, K. and Lucas, N. 2001. Using ArcGIS Geostatistical Analyst. *Redlands: ESRI*.
- Joseph, S., Reddy, C. S., Thomas, A. P., Srivastava, S. K., and Srivastava, V. K. 2010. Spatial interpolation of carbon stock: a case study from the Western Ghats biodiversity hotspot, India
- Kazemi, S. M., and Hosseini, S. M. 2011. Comparison of spatial interpolation methods for estimating heavy metals in sediments of Caspian Sea. *Expert Systems with Applications*, 38, 1632-1649.
- Keller, B. J., Back, R. C., Westrick, J., Werner, M., Evans, B., Moerke, A., Zimmerman, G. Wright, D. D., Grenfell, E., and Courneya, J. 2011. Sediment quality at select sites in the St. Marys River Area of Concern. *Journal of Great Lakes Research*, 37, 12-20.

- Lam, N. S. N., 1983. Spatial interpolation methods: a review. *American Cartographer* 10, 129-149.
- Lambert, T. W., Boehmer, J., Feltham, J., Guyn, L., and Shahid, R. 2011. Spatial Mapping of Lead, Arsenic, Iron, and Polycyclic Aromatic Hydrocarbon Soil Contamination in Sydney, Nova Scotia: Community Impact from the Coke Ovens and Steel Plant. *Environmental and Occupational Health*, 6(3), 128-145.
- Li, J., and Heap, A. D. 2011. A review of comparative studies of spatial interpolation methods in environmental sciences: Performance and impact factors. *Ecological Informatics*, 6, 228-241.
- Li, J., Heap, A. D., Potter, A., Huang, Z., and Daniel, J. J. 2011. Can we improve the spatial predictions of seabed sediments? A case study of spatial interpolation of mud content across the southwest Australian margin. *Continental Shelf Research*, 31, 1365-1376.
- Li, J., Lu, Y., Jiao, W., Wang, T., Luo, W., and Gietsy, J. P. 2010. Polycyclic aromatic hydrocarbons in soils of an industrial area of China: multivariate analyses and geostatistics. *Chemistry and Ecology*, 26(1), 35-48.
- Moerke, A. H., and Werner, R. M. 2011. Ecological status of the St. Marys River: Forward. *Journal of Great Lakes Research*, 37, 1-4.
- Nichols, S. J., Manny, B. A., Schloesser, D. W., and Edsall, T. A. 1991. Heavy metal contamination of sediments in the Upper Connecting Channels of the Great Lakes. *Hydrobiologia*, 219, 307-315.
- Palmer, D. J., Hock, B. K., Kimberly, M. O., Watt, M. S., Lowe, D. J., and Payn, T. W. 2009. Comparison of spatial prediction techniques for developing *Pinus radiata* productivity surfaces across New Zealand. *Forest Ecology and Management*, 258, 2046-2055.
- Remedial Action Plan (RAP). 1992. St. Marys River Area of Concern Environmental Conditions and Problem Definitions. Remedial Action Plan Stage 1. *Ontario Ministry of the Environment and the Michigan Department of Natural Resources*.
- Remedial Action Plan (RAP). 2002. Stage 2: Remedial Strategies for Ecosystem Restoration. *Environment Canada, US Environmental Protection Agency, Ontario Ministry of the Environment, Michigan Department of Environmental Quality*.
- Ripley, M. P., Arbic, B., and Zimmerman, G. 2011. Environmental history of the St. Marys River. *Journal of Great Lakes Research*, 37, 5-11.
- Rodriguez, P. 2009. Assessing the Geographic Distribution of Mercury and Lead in Buffalo River Sediments. *Unpublished Master of Spatial Analysis Major Research Paper: Department of Geography, Ryerson University*.

- Salihoglu, G., Salihoglu, N. K., Aksoy, E., and Tasdemir, Y. 2011. Spatial and temporal distribution of polychlorinated biphenyl (PCB) concentrations in soils of an industrialized city in Turkey. *Journal of Environmental Management*, 92, 724-732.
- Sault Ste. Marie Region Conservation Authority. 2012. *Remedial Action Plan*. Retrieved from <http://www.ssmrca.ca/st-marys-river/remedial-action-plan>
- Shepard, D. 1968. A two-dimensional interpolation function for irregularly-spaced data. *Proc. 23rd National Conference ACM, ACM*, 517-524.
- Solla, S. R., and Martin, P. A. 2008. PCB accumulation in osprey exposed to local sources in lake sediment. *Environmental Pollution*, 157, 347-355.
- Sower, G. J. and Anderson, K. A. 2008. Spatial and Temporal Variation of Freely Dissolved Polycyclic Aromatic Hydrocarbons in an Urban River Undergoing Superfund Remediation. *Environmental Science Technology*, 42, 9065-9071.
- Upper Great Lakes Connecting Channel Study (UGLCCS), 1988. *Upper Great Lakes Connecting Channel Study. Volume II*. Jointly prepared by U.S. Fish and Wildlife Service, Ontario Ministry of Environment, Michigan Department of Natural Resources, Ontario Ministry of Natural Resources, Department of Fisheries and Oceans, National Oceanic and Atmospheric Agency.
- Venkatesan M. I., Merino, O., Baek, J., Northrup, T., Sheng, Y., and Shisko, J. 2010. Trace organic contaminants and their sources in surface sediments of Santa Monica Bay, California, USA. *Marine Environmental Research*, 69, 350-362.
- Xie, Y., Chen, T., Lei, M., Yang, J., Guo, Q., Song, B., and Zhou, X. 2011. Spatial distribution of soil heavy metal pollution estimated by different interpolation methods: Accuracy and uncertainty analysis. *Chemosphere*, 82, 468-476.